Mechanisms of Self-Diffusion of Linear Associative Polymers Studied by Brownian Dynamics Simulation

*Ameya Rao,[1] Jorge Ramírez,[2] and Bradley D. Olsen[1]**

[1]Department of Chemical Engineering, Massachusetts Institute of Technology, Cambridge, MA 02139

[2]Department of Chemical Engineering, Universidad Politécnica de Madrid, Madrid, Spain

*Corresponding Author
Bradley D. Olsen
Tel: (617) 715-4548
Email: bdolsen@mit.edu

For Table of Contents Use Only

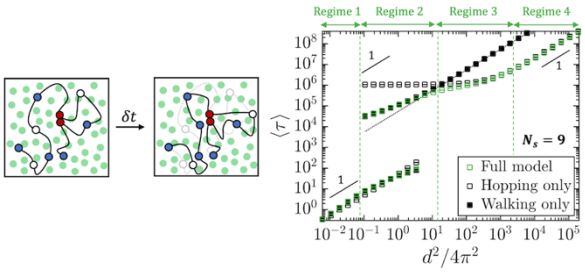

ABSTRACT: Anomalous self-diffusive behavior in associative polymer gels has been attributed to the presence of multiple diffusive mechanisms on different length scales; however, the role of these dynamic modes in networks of linear polymers with pendant stickers remains unknown, particularly at sticker densities below the mean-field limit. Here, a generalized Brownian dynamics model is developed to study the effect of transient binding on self-diffusion of unentangled linear polymers with regularly spaced stickers, selected as a prototypical associative network model with wide experimental relevance. The simulations reveal an interplay between several diffusive mechanisms, including segmental fluctuations, "walking" diffusion, and "hopping" diffusion, each governed by a molecule's connectivity to the network. These dynamic modes combine to result in multiple self-diffusive regimes on different length scales, including two distinct regimes of apparent superdiffusion before terminal Fickian diffusion, consistent with experiment. The two superdiffusive regimes have different physical origins: while one occurs due to a transition from walking to hopping, the second occurs from walking alone on smaller length scales, even in the absence of hopping. This second superdiffusive regime is proposed to arise from an increase in the chain pervaded volume upon sticker detachment, which increases the walking step size compared to the "cage" formed by binding. Each self-diffusive regime is highly sensitive to the sticker concentration, equilibrium constant, and association/dissociation kinetics due to their effects on the walking and hopping modes. Notably, increasing a chain's sticker density promotes intramolecular loops and enables superdiffusive scaling through hopping; in contrast, increasing the chain concentration promotes intermolecular binding and suppresses hopping, resulting in dynamics approaching the mean-field limit of Fickian center-of-mass diffusion on all length scales. Analytical predictions for the hopping and walking diffusivities demonstrate a link between the

static network structure, bond lifetime, and contribution of each dynamic mode, with qualitative agreement with simulation.

1. INTRODUCTION

Knowledge of dynamics in associative macromolecular networks is centrally important for understanding biophysical processes and designing soft materials for applications spanning drug delivery, tissue engineering, and organic electronics.[1–3] In associative materials, the network structure is primarily held together by weak physical interactions such as hydrogen bonding,[4] metal-ligand coordination,[5] and hydrophobic aggregation[6] between macromolecules with bond lifetimes on the order of $\sim 1 - 1000$ seconds,[5,7,8] wherein the reversible nature of the bonds allows junction exchange and molecular self-diffusion on length scales larger than the radius of gyration.[9,10] This interplay between sticker association and molecular transport gives rise to dynamic properties crucial to biophysical processes such as selective protein translocation through the nuclear membrane[11–13] and homologous recombination of DNA,[14] as well as synthetic soft material functionalities such as stimuli-responsiveness, stress relaxation, and self-healing abilities.[15–21] In all cases, understanding the internal molecular dynamics on different length scales, particularly the self-diffusive dynamics of the network-forming chains, is essential for predicting a system's collective behavior and optimizing its performance for various applications.

Transient network theory has emerged as a powerful tool to understand associative network behavior, using mean-field approaches to predict macroscopic properties such as the shear modulus, viscosity, and relaxation time from molecular-scale parameters such as the association energy, bond lifetime, and polymer chain length.[22–27] For a prototypical network formed by linear polymers with multiple associative side-groups, these theories have established the pivotal role of the stickers in increasing the local friction of a chain, resulting in a strong effect of sticker density

and polymer concentration on overall network dynamics.[24,28] However, though theoretical efforts have found success in predicting the bulk rheological behavior of associative systems,[5,29–32] their ability to accurately capture self-diffusive dynamics has not been verified to similar depth. Recent experiments have shown that associative polymers with relatively few (~10) stickers per chain, both in linear and branched architectures, can exhibit unexpected self-diffusive behavior on different length scales, including apparent superdiffusion on length scales ~10-1000 times the radius of gyration.[29,30,33,34] These anomalous dynamics have been proposed to arise due to the coexistence of multiple diffusive modes, which are largely not considered by current theories, including bound-state diffusion (e.g., "walking") and relatively free diffusion by complete detachment of all stickers from the network ("hopping").[13,35–37] Mechanisms involving correlated sticker or chain motion in large clusters have also been proposed, though their role in quiescent-state dynamics is unclear.[24,30,36–38] The hopping mechanism, in particular, has been suggested to enable superdiffusive scaling in end-functionalized 4-arm star molecules when the sticker association kinetics are slower than the conformational relaxation rate of the star arm.[37]

For the general case of linear polymers with associative side-groups,[24,25,29,39] the presence and contribution of these diffusive modes toward network dynamics remain largely unknown. Theoretical studies of linear associative polymers have focused on the limiting case of high sticker density, leading to a mean-field prediction of Rouse-like relaxation and purely Fickian diffusion on all length scales.[24,25,28,32] These theories largely do not consider the interplay between different diffusive mechanisms and assume negligible hopping in the high-sticker-density limit. Experimental evidence, however, suggests that hopping may be a significant diffusive mode in linear polymers even when the number of stickers is increased to 15 per chain,[29] a surprising observation given the small likelihood of simultaneous detachment of such many binding groups.

The ability for linear polymers to form complex topological structures due to intramolecular binding (e.g., loops of various orders)[40] may enhance the likelihood of hopping or lead to alternative roles of each diffusive mechanism compared to end-functionalized molecules such as the 4-arm stars.[34,37,41] Further study of polymers with different sticker densities, particularly sticker densities below the mean-field limit, is required to understand the contributions of the individual dynamic modes toward self-diffusive behavior as a complement to the theoretical treatments to date.[24,25,28]

In this work, a generalized Brownian dynamics model of gel-forming linear polymers with a finite number of pendant stickers is developed to explore the effect of transient binding of self-diffusion over a wide range of length scales, from less than the radius of gyration up to the macroscopic Fickian regime. The simulations reveal an interplay between dynamic modes of segmental fluctuations, walking diffusion, and hopping diffusion that results in two distinct regimes of superdiffusive scaling, each with a different origin. The effect of cross-link density in the network is explored by varying the chain concentration, number of stickers per chain, and binding equilibrium constant, resulting in differences in topological structure that enable superdiffusive behavior via hopping even at high sticker density. A comparison of the simulations with experimental self-diffusion measurements of analogous associative polymers[29,33] finds qualitative agreement, suggesting that this molecular model can successfully capture key dynamic behaviors of various associative systems across a range of length scales.

2. MODEL AND METHODS

The bead-spring model developed here is a hybrid Brownian dynamics/Monte Carlo model where chain motion is governed by Langevin dynamics and sticker binding/unbinding events are handled through a kinetic Monte Carlo scheme, similar to previous studies.[37,39,42] Each simulation

contains $n = 500$ chains of $N = 49$ beads connected by springs of Kuhn length b dispersed in a constant volume V. In semi-dilute conditions in a good solvent, strands between stickers can be modeled as freely-jointed chains of correlation blobs undergoing Rouse motion, where long-range interactions such as excluded volume and hydrodynamic forces are screened on length scales larger than the correlation blob size.[43] The number of beads $N = 49$ per chain is selected to allow various numbers of evenly spaced stickers along the chain while keeping the total chain length constant. Each bead-spring unit represents a subsection of the chain with enough monomers to have Gaussian conformational statistics; thus, the total number of monomers per chain is representative of typical degrees of polymerization of associative polymers studied experimentally. Each bead has friction factor ξ, and adjacent beads along the chain interact via a Hookean spring potential $U_s(\Delta r) = 3k_BT\Delta r^2/2b^2$, where Δr is their separation distance, k_B is Boltzmann's constant, and T is temperature. For all simulations, the length b and relaxation time $\tau_s = b^2\xi/k_BT$ of a single Kuhn segment are chosen as the units of length and time, respectively.

On each chain, N_s beads are designated as stickers; these sticker beads are identical to normal beads except that they can form transient intermolecular or intramolecular bonds, as described below. Stickers are placed on each end and spaced regularly along the chain, such that the number of springs between stickers is $\Delta N_{strand} = (N-1)/(N_s-1)$. Only pairwise sticker association is allowed, analogous to experimental systems based on hydrogen bonding[4,44] and metal-ligand coordination.[5,7] To access a wide range of time scales, chains are conceptualized as diffusing through a structureless, unentangled gel medium with sticker association treated in a mean-field sense (see Fig. 1). Therefore, pairwise interactions between different chains are not explicitly considered in this work, reducing computational cost. It is important to note that this treatment of the gel as a structureless medium is intended to capture the essential physics of the

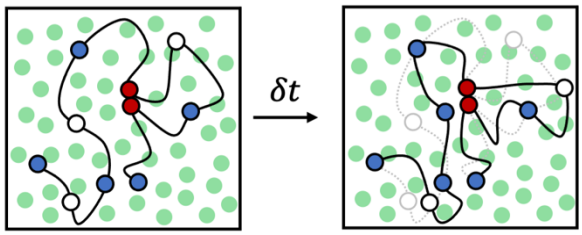

Figure 1. Schematic representation of the simulation model, illustrating a chain with regularly spaced stickers diffusing through a structureless medium while forming transient bonds with the mean-field background. The mean-field background is composed of binding sites (green dots) representing the state of all stickers in the system. Intermolecularly bound stickers (blue dots) are attached to the background and held fixed in place, while intramolecularly bound stickers (red dots) are constrained to move together as a rigid body but not attached to the background. Free stickers (white dots) are also not attached to the background and free to fluctuate as any non-sticky bead. The two panels show an example of one time step δt in the simulation. In the right-hand side panel, the chain's initial position is shown in faded color for comparison.

gel matrix, particularly the total sticker density, but it neglects network inhomogeneities and geometric constraints on certain length scales that may affect the chain conformational and sticker binding statistics through entropic effects.[35,36]

Chain trajectories are calculated by solving the overdamped Langevin equation in three dimensions, where the position of bead j on molecule i is governed by

$$\xi \frac{\delta \boldsymbol{r}_{i,j}}{\delta t} = \frac{3k_B T}{b^2}\left(\boldsymbol{r}_{i,j+1} + \boldsymbol{r}_{i,j-1} - 2\boldsymbol{r}_{i,j}\right) + \boldsymbol{F}_{B(i,j)} \tag{1}$$

The random Brownian force $\boldsymbol{F}_{B(i,j)}$ is selected in each dimension from a Gaussian distribution with zero mean and variance $2k_B T\xi/\delta t$ for discretized time step δt. As chains diffuse, they can form transient intermolecular or intramolecular bonds (forming a bridge or loop, respectively) or, if already bonded, dissociate from an existing bridge or loop. Intermolecular association is considered to occur with a mean-field background, where any pair of stickers can form a virtual bond irrespective of their relative positions in real space. Intermolecularly bound stickers are held fixed in place, i.e., $\delta \boldsymbol{r}_{i,j}/\delta t = 0$, with fluctuations of intermolecular junctions not studied in this work. Intramolecularly bound sticker pairs on the same chain are constrained to move together as a rigid body with total friction 2ξ, with the intramolecular bond length held equal to the sticker

pair's instantaneous separation distance upon forming the loop. That is, if bead j is intramolecularly bonded to bead k, the elastic and Brownian forces acting on bead k are added to the right-hand side of the governing equation for $\boldsymbol{r}_{i,j}$, and its friction factor is set to 2ξ. Similarly, the elastic and Brownian forces acting on bead j are added to the governing equation for $\boldsymbol{r}_{i,k}$, and its friction factor is also set to 2ξ. This transmission of forces effectively places an infinitely stiff spring between each looped sticker pair, causing the two beads to act as a single rigid body with a constant bond length without altering the total friction of the chain (see Section 1f of the Supporting Information for validation).

Sticker association reactions are implemented via stochastic chemical kinetics, where the probability of each reaction g at each time step is governed by a propensity function α_g that considers the association states of all the stickers in the system.[45] In this work, sticker binding and unbinding reactions are considered to follow second- and first-order kinetics, respectively. The total intermolecular binding propensity is

$$\alpha_I = \frac{k_A}{V}\sum_{i=1}^{n} f_i(F - f_i) \tag{2a}$$

where k_A is the association rate constant, V is the system volume, f_i is the number of free stickers on molecule i, and F is the total number of free stickers in the system. The propensity for intramolecular association (forming a loop) is

$$\alpha_L = \sum_{i=1}^{n}\sum_{j\neq k}^{N_s} \frac{k_A}{4\pi R_{cutoff}^3/3} l_{ijk} \tag{2b}$$

where R_{cutoff} is a cutoff distance and l_{ijk} is a Boolean variable that is 1 if both stickers j and k are available to bind and $\left|\boldsymbol{r}_{i,j} - \boldsymbol{r}_{i,k}\right| < R_{cutoff}$, and 0 otherwise. Thus, only free sticker pairs whose separation distance is less than R_{cutoff} (chosen to be $0.1b$, as described below) are

considered for intramolecular binding, and the reaction probability is independent of their separation distance once below this threshold. This treatment of intramolecular association allows both the total bound sticker fraction and the loop fraction to be predicted analytically and results in the total looping propensity being independent of R_{cutoff} provided that R_{cutoff} is small, with truncation error of $O(R_{cutoff}^2)$ as shown in the Supporting Information. Finally, the propensity for sticker dissociation is

$$\alpha_D = k_D \left(\frac{nN_s - F}{2} \right) \tag{2c}$$

where k_D is the dissociation rate constant and $(nN_s - F)/2$ is the total number of bonds in the system. The association and dissociation rate constants are related through the binding equilibrium constant, $K_{eq} = k_A/k_D$.

The overdamped Langevin equation (Eq. 1) was integrated using a modified 4th-order Runge-Kutta scheme previously described by Spakowitz and coworkers.[46] At every time step, the association states of the stickers were updated using the tau-leap algorithm,[47] where the number of occurrences of each reaction g (intermolecular association, intramolecular association, and dissociation) were drawn from a Poisson distribution with mean and variance equal to $\alpha_g \delta t$, with α_g being the reaction propensity in Eq. 2. Since the probabilities of all reactions of the same type are equal, the actual stickers to react were selected randomly from all possible candidates for each reaction. A constant time step of $\delta t = 0.1\tau_s$ was used for most simulations, chosen to ensure both accurate integration of the Langevin equation using the RK4 scheme and fidelity to the leap condition mandating that all reaction propensities remain essentially constant during a time step.[47,48] In particular, the formulation of the looping propensity in this model (Eq. 2b) requires the time step to scale with R_{cutoff}^3/k_A in order to avoid the number of intramolecular reactions

exceeding the number of available candidate pairs at any time step. The cutoff distance for intramolecular binding was chosen to be $R_{cutoff} = 0.1b$ for all simulations in this work to represent a physically realistic bond without requiring an excessively small time step for the range of k_A investigated. For most simulations, the value of k_A used did not require the time step to be lower than $\delta t = 0.1\tau_s$, as determined using a conservative estimate for the maximum time step satisfying the leap condition (see Section 1d of the Supporting Information). For the few simulations in which a larger value of k_A was used, the time step was lowered in proportion to k_A^{-1} to ensure fidelity with the leap condition for the intramolecular propensity. Specifics related to the validation of the simulation model and choice of time step are discussed in detail in Section 1 of the Supporting Information.

Table 1 lists the seven associative linear polymers that were simulated in this work, each with a different number of stickers per chain, N_s. All polymers had the same total length of $N = 49$ beads. The minimum concentration for formation of a percolating network is the chain overlap concentration at which $V = nV_{span}$, where $V_{span} = 4\pi(Nb^2/6)^{3/2}/3$ is the characteristic volume spanned by a Gaussian chain. Normalizing the concentration by the overlap concentration, a dimensionless concentration was defined as $\phi = nV_{span}/V$, where $\phi = 1$ at overlap. All simulations were run at $\phi \geq 1$ to be physically realistic. The equilibrium constant was chosen to be $K_{eq} > 1$ for all simulations to capture the favorable binding in experimental associative systems such as those based on coiled-coil aggregation[30,33,35,36] and metal-ligand coordination.[7,34,41] In addition, for most simulations the sticker association rate was chosen to be slow compared to the Rouse time of the chain (i.e., $k_A\langle F\rangle/V \ll (N^2\tau_s)^{-1} = 1/48^2$ in the simulation units, where $\langle F\rangle$ is the average number of free stickers in the system). This separation in timescales is characteristic of a kinetics-limited system,[39] which applies to a large majority of experimental associative

polymer gels[9,33] and is hypothesized to be crucial in enabling chain superdiffusive behavior via hopping.[37]

All simulations were run at equilibrium, with the average chain conformations and sticker association states constant over time (to within fluctuations governed by the system size). Simulations were equilibrated in two stages before each run. In the first stage, simulations were initialized by generating a Gaussian chain conformation for each molecule with all stickers initially unbound. Then the system was allowed to evolve to the equilibrium distribution of chain conformations and sticker association states until the free sticker fraction, loop fraction, and mean-square chain end-to-end distance became constant over time. In the second stage of equilibration, the system was allowed to evolve further until the chain end-to-end vector autocorrelation function decayed to zero (to within the noise), indicating relaxation of the system. Representative plots of each stage of the equilibration procedure are shown in the Supporting Information in Section 1f. During each simulation run, time-correlation functions including the center-of-mass mean-square displacement and self-intermediate scattering function were calculated from snapshots taken every 10 time steps and stored.

Table 1. Associative linear bead-spring chains studied in this work. Each chain has 49 beads in total.

Number of stickers (N_s)	**Number of springs between stickers (ΔN_{strand})**
4	16
7	8
9	6
13	4
17	3
25	2
49	1

3. RESULTS AND DISCUSSION

To facilitate comparison with common diffusion measurements based on light and neutron scattering,[30,33,49,50] Fig. 2a presents representative profiles of the center-of-mass self-intermediate scattering function $S_{inc}(q,t)$ for various wavevectors q from a simulation with $N_s = 4$ stickers per chain, with simulation parameters of $K_{eq} = 15$, $k_A = 0.0002$, and $\phi = 1$. The simulation parameters were chosen to ensure strong sticker binding ($K_{eq} > 1$) and slow association kinetics compared to the Rouse relaxation time of the chain ($k_A\langle F\rangle/V \ll (N^2\tau_s)^{-1}$). This separation of timescales is characteristic of a kinetics-limited system,[39] which has been shown to be relevant to most experimental associative polymer gels[9,33,36] and hypothesized to be crucial in enabling chain superdiffusive behavior via hopping.[37] The self-intermediate scattering function is the Fourier transform of the single-chain position correlation function:

$$S_{inc}(q,t) = \frac{1}{n}\sum_{i=1}^{n}\langle \exp(i\boldsymbol{q}\cdot[\boldsymbol{r}_i(t) - \boldsymbol{r}_i(0)])\rangle \tag{3}$$

where $\boldsymbol{r}_i(t)$ is the center-of-mass position of chain i at time t. Averages were performed over different starting times and over orthogonal directions of $\boldsymbol{q}$. The temporal evolution of $S_{inc}(q,t)$ informs on self-diffusive chain motion on the length scale $d = 2\pi/q$. As shown in Fig. 2a, $S_{inc}(q,t)$ shows qualitatively different behavior depending on the length scale probed, transitioning from a single exponential decay on small length scales to a two-mode relaxation for intermediate length scales ($0.2b^2 \lesssim d^2/4\pi^2 \lesssim 1000b^2$) until again returning to a single exponential on large length scales. The relaxation curve for each wavevector was fit to a double stretched exponential function of the form

$$S_{inc}(q,t) = A\exp\left[-\left(\frac{t}{\tau_{fast}}\right)^{\beta_{fast}}\right] + (1-A)\exp\left[-\left(\frac{t}{\tau_{slow}}\right)^{\beta_{slow}}\right] \tag{4}$$

where the time constants were defined such that $\tau_{slow} > \tau_{fast}$, and the amplitude parameter A varied between 0 and 1 depending on the relative contribution of each mode. For intermediate values of d^2 where a two-mode relaxation is observed, the stretching parameters β_{fast} and β_{slow} range between 0.7 and 1, indicating heterogeneity in each relaxation process. However, for both small and large values of d^2 where the relaxation profile exhibits only a single mode, the stretching parameter is greater than 0.95, consistent with a homogeneous diffusive process.

In Fig. 2b, the average relaxation times of the intermediate scattering function, $\langle\tau_{fast}\rangle$ and $\langle\tau_{slow}\rangle$, are examined as a function of the reduced diffusion length scale, $d^2/4\pi^2$. Relaxation times were computed as the first moment of the relaxation distribution of each mode, $\langle\tau_i\rangle = \frac{\tau_i}{\beta_i}\Gamma\left(\frac{1}{\beta_i}\right)$, where Γ is the Gamma function. For Fickian diffusion, the decay of each mode i should follow a simple exponential $S_{inc}(q,t) \sim \exp(-t/\tau_i)$, where time constant τ_i is proportional to d^2 via the diffusion coefficient, $D_i = d^2/4\pi^2\langle\tau_i\rangle$. As seen in Fig. 2b, the relaxation behavior of $S_{inc}(q,t)$ exhibits several non-Fickian regimes which can be parameterized for each mode by the relationship $\langle\tau_i\rangle \sim d^{2\mu}$. The dynamics of the linear 4-sticker polymers shown here share similar qualitative features with recent simulations of telechelic 4-arm stars,[37] including an early-time Fickian regime ($\mu = 1$) for the fast mode (Regime 1) and apparent superdiffusive scaling ($\mu < 1$) for the slow mode on intermediate length scales (Regimes 2 and 3) before the onset of terminal Fickian diffusion (Regime 4). It is important to note that the relationship $\langle\tau_i\rangle \sim d^{2\mu}$ is different than the classical expression of mean-square displacement over time, $\langle\Delta R^2\rangle \sim t^{\alpha}$, with the scaling exponents related via $\mu = 1/\alpha$. Thus, $\mu < 1$ is equivalent to $\alpha > 1$, indicating apparent

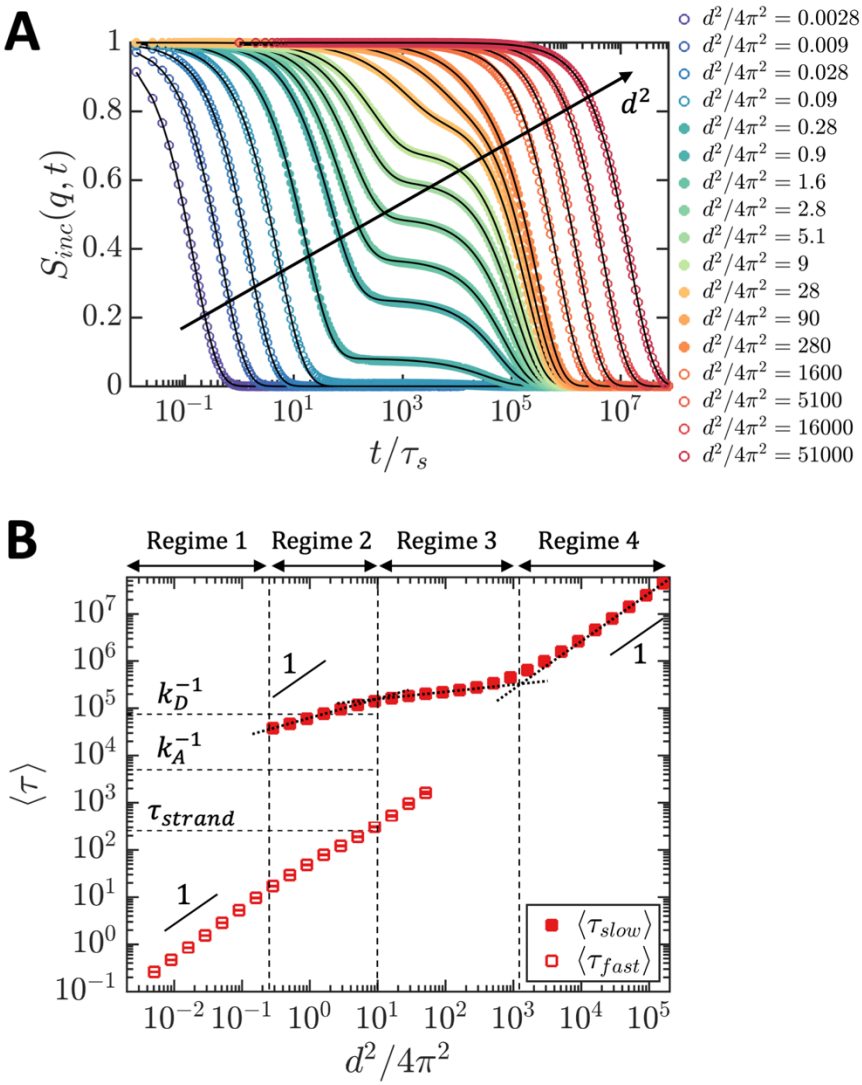

Figure 2. (A) Representative relaxation profiles of the self-intermediate scattering function $S_{inc}(q,t)$ for various values of $d^2/4\pi^2 = 1/q^2$ from a simulation of linear 4-sticker chains with $N = 49$ beads total, with $\phi = 1$, $K_{eq} = 15$, and $k_A = 0.0002$. Solid lines are a fit to either a single exponential or sum of two exponentials, defined in the text in Eq. 4. Open symbols indicate a single-mode relaxation and closed symbols indicate a two-mode relaxation. (B) Mean relaxation time constants of $S_{inc}(q,t)$ as a function of d^2. Error bars are 95% confidence intervals for the fits to Eq. 4 (and if not visible are within the marker). The horizontal dashed lines denote the characteristic timescales of the system, including the sticker association and dissociation times (k_A^{-1} and k_D^{-1}, respectively) and the strand Rouse relaxation time $\tau_{strand} = \Delta N_{strand}^2 \tau_s$. The vertical dashed lines indicate transitions between the diffusive regimes observed at different length scales, labeled numerically on the top. Dotted lines are power-law fits $\langle\tau_{slow}\rangle \sim (d^2)^{\mu}$ for Regimes 2-4, where $\mu = 1$ for Fickian diffusion and $\mu < 1$ for apparent superdiffusion. Units of length and time are the single-spring Kuhn length b and relaxation time τ_s, respectively.

superdiffusive scaling. Although the superdiffusive behavior of τ_{slow} in Regime 3 in the linear 4-sticker polymers is similar to that observed in the stars, the linear polymers undergo a more pronounced second superdiffusive regime at lower d^2 (Regime 2) compared to the stars.[37] The

presence of two distinct superdiffusive regimes in the linear polymers is consistent with recent experimental measurements of linear protein self-diffusion which have suggested the coexistence of multiple mechanisms underlying superdiffusive behavior on different length scales.[33]

The regimes in Fig. 2b reflect the various relaxation processes occurring on each length and time scale. On length scales smaller than the correlation blob size (Regime 1, $d^2/4\pi^2 \ll b^2$), $S_{inc}(q,t)$ exhibits a single non-stretched exponential mode with a relaxation time τ_{fast} consistent with Fickian scaling ($\mu = 1$). This regime corresponds to segmental fluctuations of the connecting strands between stickers on time scales smaller than their Rouse relaxation time ($\tau_{strand} \approx \Delta N_{strand}^2 \tau_s = 256\tau_s$), resulting in diffusion of the center-of-mass up to a certain characteristic length scale. In this regime, relaxation times are faster than the characteristic sticker association and dissociation kinetics, and stickers can be considered permanently bound as in a covalently cross-linked gel.[33,50] The maximum length scale of the single-mode regime (before the onset of the slow mode) is governed by the maximum mean-square center-of-mass displacement of a chain at fixed sticker bonding, i.e., on time scales shorter than the sticker lifetime (governed by k_D^{-1}). This confinement due to binding creates a caging effect that hinders chain diffusion beyond the characteristic length scale d_{cage}.[37,39] However, unlike in the telechelic star polymers where the size of the cage is directly related to the arm length ($d_{cage}^2/4\pi^2 \approx \Delta N_{arm} b^2$),[37] the linear polymers undergo this caging regime on length scales significantly smaller than the strand length between stickers ($d_{cage}^2/4\pi^2 \approx 0.1b^2 \ll \Delta N_{strand} b^2$). This difference is due to the decoupling of the fluctuations of different strands in the linear polymer (since intermolecularly bound stickers are fixed in place), resulting in its relatively small mean-square center-of-mass displacement within the cage compared to a star.

On length scales larger than the size of the cage (Regimes 2-4), segmental motion alone cannot result in full relaxation of $S_{inc}(q,t)$ due to topological constraints caused by sticker binding. Here, a second slow relaxation mode is observed corresponding to center-of-mass diffusion beyond the confines of the cage, which requires the dissociation of one or more stickers. To allow comparison with common diffusion measurement techniques such as forced Rayleigh scattering,[30,33,34] the majority of the analysis in this work focuses on the behavior of the slow mode $\langle\tau_{slow}\rangle$ except for the early-time regime where only the fast mode is present. As shown in Fig. 2b, the onset of the slow mode occurs at a relaxation time approximately equal to $\frac{k_D^{-1}}{2} = \frac{75000}{2}\tau_s$, reflecting the average bond lifetime adjusted for the pairwise nature of binding (i.e., each bond dissociation event results in detachment of two stickers). On time scales greater than this dissociation time, the occurrence of multiple binding and unbinding events allows center-of-mass chain diffusion over distances larger than the size of the cage. The simulations reveal that chain diffusion over these length scales occurs primarily by two mechanisms: (1) "walking," or sequential dissociation and re-association of individual stickers on a chain to different sites in the network, and (2) "hopping," or simultaneous detachment of all of a chain's stickers from the network, enabling the chain to undergo relatively unhindered diffusion over large distances before rebinding to the network. On these intermediate length scales, the slow mode $\langle\tau_{slow}\rangle$ exhibits two distinct superdiffusive regimes (Regimes 2 and 3), each occurring over ~2 decades of d^2 and ~1 decade of τ. Finally, on long length and time scales chains transition to terminal Fickian diffusion (Regime 4) with an effective diffusivity that is constant with d^2. It is notable that in contrast to the chain relaxation behavior measured by $S_{inc}(q,t)$, a plot of the mean-square center-of-mass displacement over time does not reveal the regimes of superdiffusive scaling (Fig. S10). Instead, only a subdiffusive regime (i.e., $\langle\Delta R^2\rangle \sim t^{\alpha}$, with $\alpha < 1$) is observed between short-time and long-

time Fickian regimes, which occurs due to the caging effect caused by binding. This is because the mean-square displacement reflects only the average behavior of all diffusing species in the system, whereas the intermediate scattering function $S_{inc}(q,t)$ is sensitive to the presence of multiple diffusing populations, particularly the slow-diffusing tail of the distribution, thus enabling a more detailed view into chain dynamics on different length scales.[30,37]

Origin of superdiffusive scaling regimes. The presence of two superdiffusive regimes in Fig. 2b suggests the presence of distinct physical mechanisms that can cause superdiffusive behavior on different length scales. Prior work has proposed a transition between walking and hopping as the origin for superdiffusive scaling, where the hopping mode allows faster diffusion over long distances compared to walking.[30,33,37] To deconvolute the individual effects of each mode, simulations were performed where each diffusive mechanism (i.e., either hopping or walking) was selectively disabled. This selection was achieved by moving the frame of reference of each chain along with its center-of-mass trajectory while it underwent the diffusive mechanism to be eliminated. This ensured that the chain center of mass remained stationary (in its moving reference frame) but that its conformation and binding configuration were able to fluctuate as normal, allowing isolation of each mode without perturbing the conformational motion or sticker binding dynamics in any way.

In Fig. 3, the chain diffusion curves for the full model are compared with hopping- and walking-only models for several values of N_s. For the full model, the same four qualitative diffusive regimes are observed for all values of N_s, as shown earlier for the $N_s = 4$ case (Fig. 2b), though the transition length scales between regimes vary with N_s (see Fig. S14). Comparing the curves in each panel of Fig. 3 reveals pronouncedly different behavior in diffusion by walking and

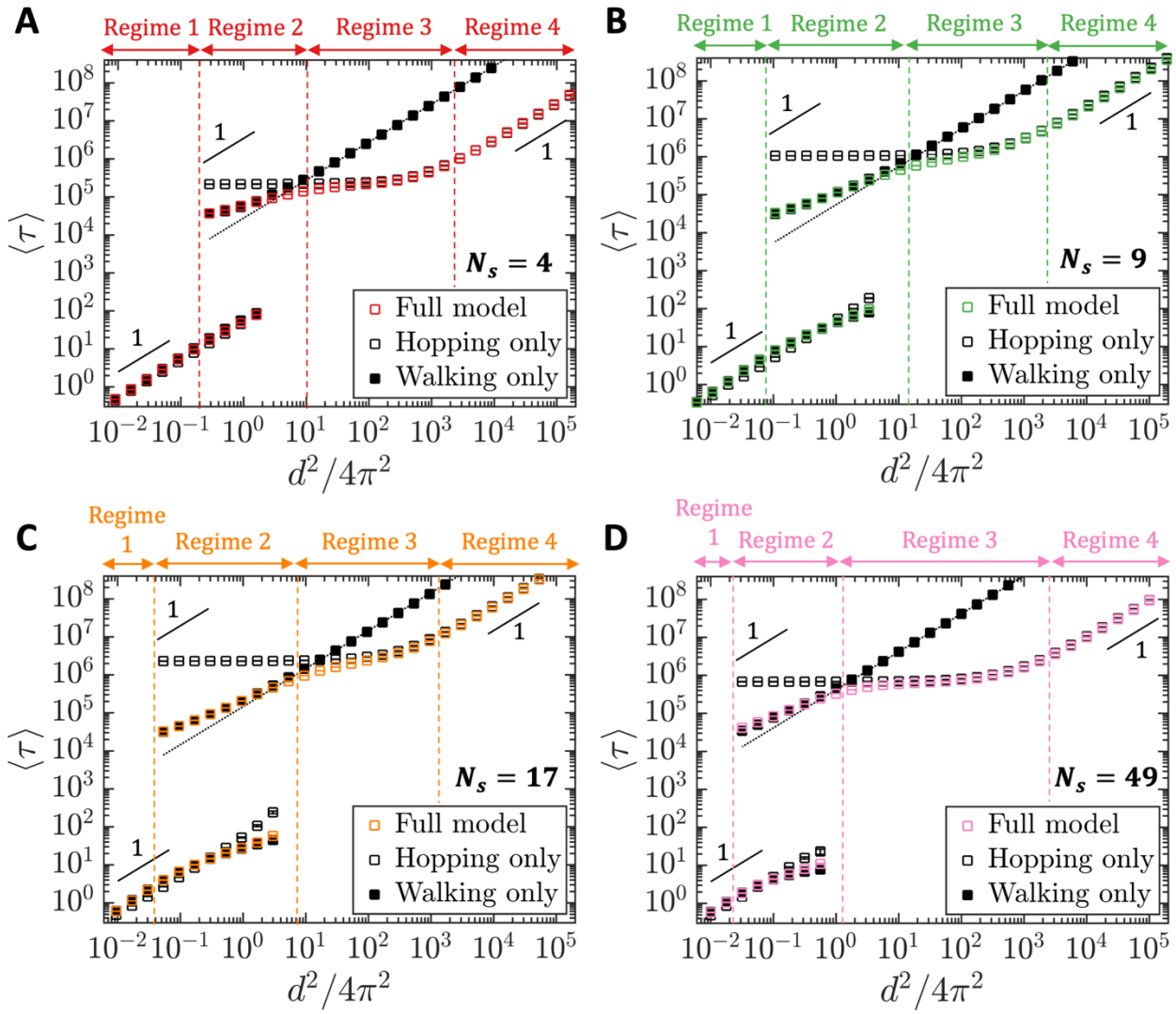

Figure 3. Comparison of chain diffusion curves in the full model and with walking and hopping individually enabled for sticker densities of (A) $N_s = 4$, (B) $N_s = 9$, (C) $N_s = 17$, and (D) $N_s = 49$ stickers per chain. The chain length is $N = 49$ beads for all simulations. Simulation parameters are $k_A = 0.0002$, $K_{eq} = 15$, and $\phi = 1$. The black dotted lines show Fickian diffusive scaling as a guide to the eye. The four diffusive regimes observed in the full model are labeled above each panel.

hopping on length scales larger than the size of the cage (i.e., in the slow time constant τ_{slow}). When only walking is enabled, chains undergo an early-time Fickian regime in the fast time constant τ_{fast} due to segmental motion, followed by the appearance of a well-separated slow mode on length scales greater than the cage size. As in the full model, the discontinuity between the fast and slow modes in the walking-only model occurs due to the large difference between the timescale of segmental diffusion (which, for length scales smaller than the cage size, can result in

full relaxation of $S_{inc}(q,t)$ even without sticker dissociation) and the bond lifetime, regardless of the absence of the hopping mode. For the slow mode in the walking-only model, chains exhibit a short regime of superdiffusive scaling before transitioning immediately to Fickian scaling with a terminal diffusivity $2-3$ orders of magnitude slower than in the full model. In contrast, when only hopping is enabled, the relaxation times of the slow mode are initially constant at small length scales before transitioning to terminal Fickian scaling with a long-time diffusivity equal to that of the full model.

A comparison between the three curves in each panel of Fig. 3 reveals two distinct mechanisms responsible for the two superdiffusive regimes seen in the full model (Regimes 2 and 3). Notably, in Regime 2 the curves for the full model and the walking-only model are quantitatively equal, demonstrating that this lower superdiffusive regime arises from walking alone. In contrast, the upper superdiffusive regime (Regime 3) results from a transition from walking to hopping, similar to the behavior seen in telechelic 4-arm stars.[37] The time scale for the transition to hopping is seen as the relaxation time plateau at low d^2 in the hopping-only model in each panel of Fig. 3, which corresponds to the average time required for a molecule to completely detach from the network. On shorter time scales, the fastest diffusive mechanism is walking since only a small fraction of molecules have had time to fully detach from the network. On longer time scales, however, the hopping mode becomes faster than the walking mode as the fraction of chains that have taken a hopping step approaches unity. The length scale associated with the transition to hopping is determined by the mean-square displacement of a molecule by walking until it begins the hopping step; it is a function of both the hopping frequency and walking diffusivity of a molecule and varies with N_s (see Fig. S14). It is important to note that the presence of superdiffusive scaling in the simulations is unlikely to arise from the lack of excluded volume and

hydrodynamic interactions in the simulation model, as these long-range interactions are screened on length scales larger than the correlation blob size and may be neglected with good accuracy in the Rouse description of unentangled chains used here.[43,51]

Examining the mean-square displacement over time with each mode deconvoluted also reveals a transition from walking to hopping for each value of N_s (Fig. S11), where the hopping mode becomes faster than the walking mode above a certain time scale (depending on the particular value of N_s). However, as in the full model, the MSD does not show signs of apparent superdiffusive scaling in any of the curves, even when hopping and walking are selectively enabled. In the walking-only model, similar to the full model, the MSD shows a subdiffusive regime separating early- and late-time Fickian regimes due to tethering from binding, whereas in the hopping-only model the MSD exhibits purely Fickian scaling over all length scales. This is again due to the greater sensitivity of the self-intermediate scattering function $S_{inc}(q,t)$ to the presence of multiple diffusing species (e.g., in the hopping-only model these species include the subset of molecules that have begun a hopping step vs. those that have not); in contrast, the mean-square displacement is sensitive only to the average. Thus, by deconvoluting the effects of walking and hopping in the system, the data for $S_{inc}(q,t)$ provide evidence for a distinct set of mechanisms underlying superdiffusive behavior in associative linear polymers, including the ability for chains to exhibit apparent superdiffusion even in the absence of hopping.

Real-space displacement distribution. The role of hopping and walking in each superdiffusive regime can be further elucidated by examining the real-space displacement distribution as chains diffuse over time. Figure 4 displays profiles of the 1D center-of-mass displacement distribution, $p(x-x_0)$, from various time snapshots from simulations of the full model and with walking and hopping each selectively enabled, with $N_s = 4$ and $K_{eq} = 15$, $k_A =$

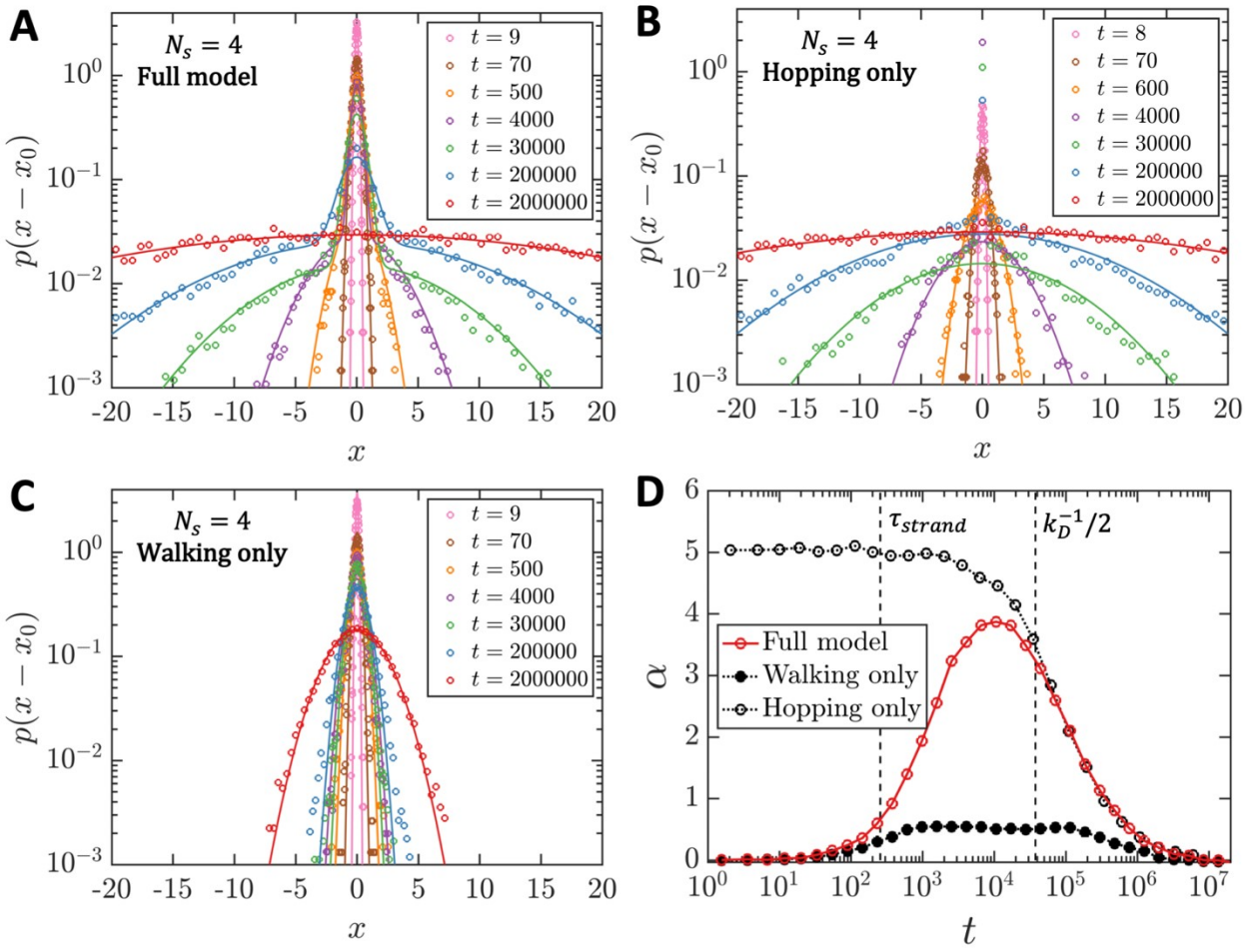

Figure 4. (A) Normalized 1D real-space distribution of the chain center-of-mass for various time snapshots of a simulation of the full model with $N_s = 4$, $k_A = 0.0002$, $K_{eq} = 15$, and $\phi = 1$. Lines are least-squares fits to sums of two Gaussians with different amplitudes and variances. (B, C) Normalized 1D real-space distributions from simulations with hopping and walking selectively enabled, respectively (all other simulation parameters identical to panel A). Lines are least-squares fits to single Gaussian functions. (D) Time evolution of the 3D non-Gaussian parameter α as defined in the text for the simulations in panels A-C. Characteristic timescales are shown for comparison.

0.002, and $\phi = 1$. For Fickian diffusion with diffusivity D_{eff}, the displacement density should be a Gaussian function with mean 0 and variance $2D_{eff}t$ in each dimension. As shown in Fig. 4a, the chain displacement distribution in the full model shows pronounced non-Gaussian behavior except for early times, $t < 100\tau_s$. This short-time regime corresponds to the Fickian diffusion observed on small length scales in Fig. 2 (Regime 1), where molecules are caged and can only diffuse via segmental motion. At later times $t > 100\tau_s$, the displacement distribution becomes bimodal and

can be captured by a sum of two Gaussian functions with different variances (solid lines in Fig. 4a). The Gaussian mode with large variance represents the population of molecules that have begun to take hopping steps and can diffuse over a large distance, whereas the second mode with small variance represents the population of molecules that have only undergone slow diffusion by walking and internal strand fluctuations. As time progresses, the fraction of molecules that have taken a hopping step increases, and the amplitude of the large-variance mode grows. Finally, at long times ($t \gtrsim 10^6 \tau_s$) the chain displacement distribution can again be captured by a single Gaussian function, which is governed by the hopping mode as the fraction of molecules that have taken a hopping step approaches 1. In contrast to the full model, when hopping and walking are selectively enabled (Figs. 4b and 4c), the displacement distributions show a smaller extent of non-Gaussian behavior and can be approximately fit with a single Gaussian function for all times. The Gaussian distributions seen in the hopping- and walking-only models (Figs. 4b and 4c) are qualitatively similar to the respective high- and low-variance modes in the full model (Fig. 4a), reflecting the individual contributions of each population of chains toward overall self-diffusion in the system.

For each model, the time scales corresponding to transitions between the single- and double-mode distributions can be quantified by examining the temporal evolution of the 3D non-Gaussian parameter,[37,39]

$$\alpha = \frac{3\langle \Delta r^4 \rangle}{5\langle \Delta r^2 \rangle^2} - 1 \tag{5}$$

where Δr is the molecule's 3D center-of-mass displacement. A value of $\alpha = 0$ indicates a single-Gaussian profile, whereas a value of $\alpha > 0$ indicates the presence of multiple populations with different diffusivities.[39,52] As seen in Fig. 4d, at both short and long times in the full model ($t < 30\tau_s$ and $t > 4 \times 10^6 \tau_s$) the non-Gaussian parameter is close to 0, indicating a single Gaussian

distribution. However, at intermediate times the value of α becomes positive, corresponding to the presence of distinct Gaussian modes from the walking and hopping populations. In contrast, in the walking-only model the non-Gaussian parameter is significantly closer to 0 for all times, consistent with the presence of only one main diffusive mechanism on length scales larger than the size of the cage. However, there is still a region of positive values of the non-Gaussian parameter over approximately the same times as in the full model, revealing a smaller but nonzero deviation from Gaussian behavior even in the absence of hopping. This positive value of α is likely related to an interplay between multiple walking modes, as seen in the superdiffusive behavior in Regime 2. Finally, in the hopping-only model, the non-Gaussian parameter has a large initial value of $\alpha = 5$ before gradually decreasing until it aligns with the long-time behavior of the full model ($t > 10^5\tau_s$). This qualitatively distinct behavior in the hopping-only model arises from the large difference between the diffusivities of the hopping molecules and those that are still attached to the network (and thus are held completely immobile, i.e., without undergoing diffusion by segmental fluctuations), which results in a large value of α on short time scales. It should be noted that in the full model, unlike in the hopping-only model, chains that are attached to the network still undergo segmental motion on short time scales, resulting in an initial bound diffusivity approximately equal to that of the hopping diffusivity and thus a small early-time value of $\alpha \approx 0$ (see Fig. 3). On long time scales where hopping dominates chain diffusion, the non-Gaussian parameters for the full and hopping-only models become quantitatively equal as they both decrease to 0. Importantly, a comparison between the Figs. 3 and 4 reveals that the timescales corresponding to non-Gaussian behavior in the real-space displacement distribution ($\alpha > 0$) correlate with those where chains undergo anomalous scaling in τ vs d^2 (Regimes 2 and 3). In contrast, the early and late times where only a single Gaussian mode is observed correlate with purely Fickian scaling

(Regimes 1 and 4). Thus, the real-space distributions are able to reveal the contributions of walking and hopping toward chain diffusion on different length scales, in particular showing that non-Gaussian behavior in the spatial distribution can occur even in the presence of only one diffusive mechanism.

Origin of superdiffusive behavior from walking. A qualitative explanation for superdiffusive scaling from walking alone (Regime 2) can be found by considering the change in the pervaded volume of strands on a chain during its transition from being caged to undergoing a walking step (i.e., before and after unbinding a sticker, which releases the topological constraint on the chain). If chains exhibited purely Fickian diffusion on all length scales beyond the cage, a limiting terminal diffusion coefficient (D_{lim}) would arise governed by the characteristic length and time scales of the exit from the cage, as shown by the dotted lines in Fig. 5a:

$$D_{lim} = 2k_D\left(\frac{d_{cage}^2}{4\pi^2}\right) = 2k_D\left(\frac{\langle \Delta R_{CM,cage}^2 \rangle}{6}\right) \quad (6)$$

where $\langle \Delta R_{CM,cage}^2 \rangle$ is the mean-square center-of-mass displacement of the chain within the cage and $2k_D$ is the sticker detachment frequency (with the factor of 2 arising from the pairwise nature of binding, i.e., each dissociation event detaches two stickers). The last equality in Eq. 6 arises from the relationship between the real-space mean-square displacement and the d-spacing of the system, which is $d^2/4\pi^2 = \langle \Delta R^2 \rangle / 2n$ where $n = 3$ is the dimensionality. The presence of superdiffusive scaling from walking following exit from the cage indicates that the long-time diffusivity of the walking mechanism, D_{walk}, must be larger than D_{lim}. The walking diffusivity can be approximated[37] as the sticker detachment frequency, $2k_D$, multiplied by a chain's mean-square center-of-mass displacement within the hypothetical "cage" (i.e., due to strand motion

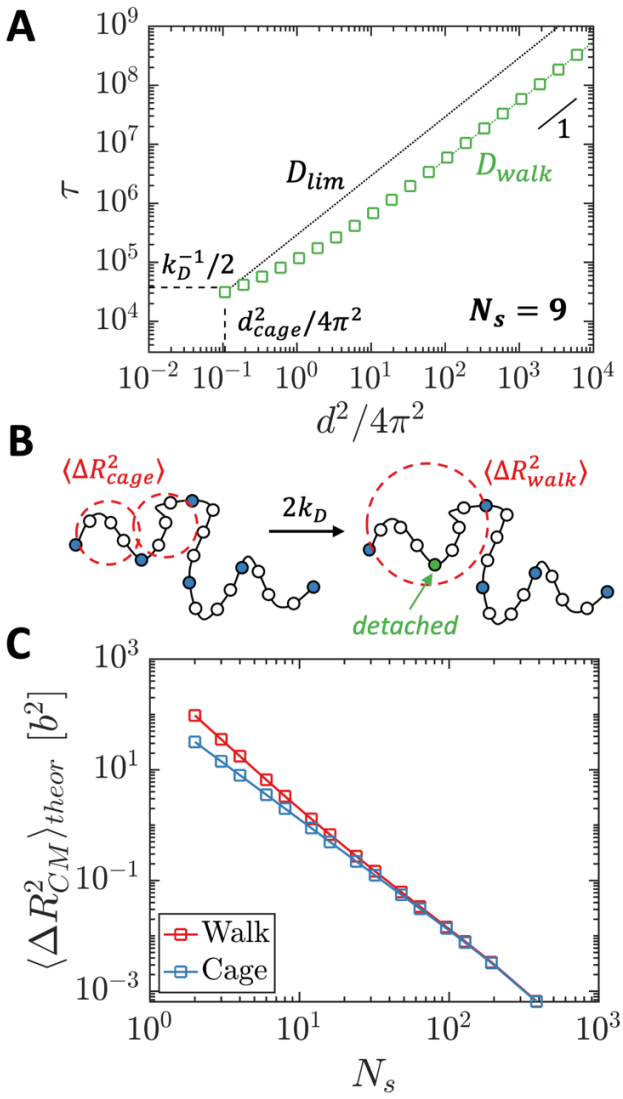

Figure 5. (A) Simulation results for the slow time constant, τ_{slow}, with hopping switched off for $N_s = 9$, $\phi = 1$, $k_A = 0.0002$, and $K_{eq} = 15$, illustrating the terminal walking diffusivity (D_{walk}) and the limiting diffusivity in the absence of superdiffusive scaling, D_{lim}. (B) Schematic representation of the increase in the strand pervaded volume upon unbinding a sticker, enabling an increase in the center-of-mass mean-square displacement during a walking step compared to within the cage. Blue filled circles are intermolecularly bound stickers, the green filled circle is the recently detached sticker, and empty circles are non-sticky beads. (C) Theoretical center-of-mass mean-square displacement (calculated as shown in the Supporting Information) of a hypothetical chain with $N = 769$ beads both within the cage and during a walking step as a function of N_s, showing a convergence with increasing N_s.

alone) resulting after unbinding a sticker, averaged over all chains and all possible sticker dissociation events:

$$D_{walk} \approx 2k_D \sum_{s=2}^{N_s} p_s \frac{\langle \Delta R^2_{CM,(s-1)} \rangle}{6} \tag{7}$$

where p_s is the probability of a chain having s attached stickers, $\langle \Delta R^2_{CM,(s-1)} \rangle$ is the mean-square center-of-mass displacement of the chain after unbinding a sticker and before rebinding, and the index s runs from 2 to N_s. The estimate for D_{walk} in Eq. 7 assumes a kinetics-limited system, where sticker dissociation is the rate-limiting step in each walking step and chains completely relax their conformation before sticker reattachment (i.e., $\tau_{strand} \approx \Delta N^2_{strand} \tau_s \ll (k_A F/V)^{-1}$). During each walking step, a chain's mean-square center-of-mass displacement, $\langle \Delta R^2_{CM,(s-1)} \rangle$, scales with the radius of gyration of each strand, $R^2_{g,strand} \approx \Delta N_{strand} b^2/6$, averaged across all strands on the chain. Because unbinding a sticker results in an increase in the average strand radius of gyration, as illustrated in Fig. 5b, the mean-square center-of-mass displacement of a chain during a walking step must *necessarily* be greater than that of the chain within the cage (i.e., before sticker unbinding). Thus, D_{walk} must be greater than D_{lim} due to the increase in the average strand length upon unbinding a sticker. The difference between D_{lim} and D_{walk} is illustrated in Fig. 5a for a simulation of a 9-sticker chain with hopping switched off, where the increase in the effective diffusivity from D_{lim} to D_{walk} is seen as the lower superdiffusive regime (Regime 2) upon exit from the cage. This analysis suggests that the lower superdiffusive regime may be a universal phenomenon in associative linear polymers due to the transition from caging to walking on timescales smaller than the onset of hopping, irrespective of sticker kinetics, equilibrium constant, or chain concentration.

However, in the limit of high sticker density where the strand length approaches zero, the impact of sticker dissociation on a chain's *average* strand length is hypothesized to be diminished due to the small spacing between stickers and the large number of strands (most of which would be unaffected by detachment of a single sticker). In turn, the extent of superdiffusive scaling from walking alone should be suppressed due the smaller change in the average strand length upon

exiting the cage. Figure 5c compares theoretical predictions for mean-square center-of-mass displacement within the cage and during a walking step (i.e., before and after detachment of a single sticker) as a function of N_s for a hypothetical long chain with 769 beads. Theoretical predictions for the mean-square displacement before and after a sticker detachment event were calculated from the configurational partition function for a Gaussian bead-spring chain with a subset of beads fixed in place, as described in Section IV of the Supporting Information. As shown in Fig. 5c, increasing N_s decreases the characteristic center-of-mass displacement both during a walking step and within the cage, resulting in a convergence of the two curves at high N_s such that $D_{lim} = D_{walk}$. It is hypothesized that superdiffusive scaling from walking may be suppressed at sufficiently high sticker density, where the characteristic walking step size becomes approximately equal to the cage size before unbinding. Although the simulations show a decrease in D_{lim} and D_{walk} with N_s that is consistent with the prediction of Fig. 5c (see Fig. S15), it is difficult to observe a clear convergence in their values due to the relatively small range of N_s accessible in the simulations. Thus, further study is required to understand the precise effect of sticker density on the extent of superdiffusive scaling from walking as seen in Regime 2.

Effect of sticker density on superdiffusive scaling by hopping. In addition to the walking diffusivity, the ability for chains to exhibit superdiffusive scaling by hopping has been hypothesized to be affected by molecular-scale parameters such as the number of stickers per chain, the association/dissociation kinetics, and the equilibrium constant.[36,37] Increasing the number of stickers per chain has been proposed to suppress hopping due to the decreased likelihood for simultaneous detachment of all stickers, which should have a strong (exponential) dependence on N_s.[37] Recent experiments, however, have suggested that hopping may be a significant diffusive mode even in polymers containing 15 stickers per chain.[29,36] To test this

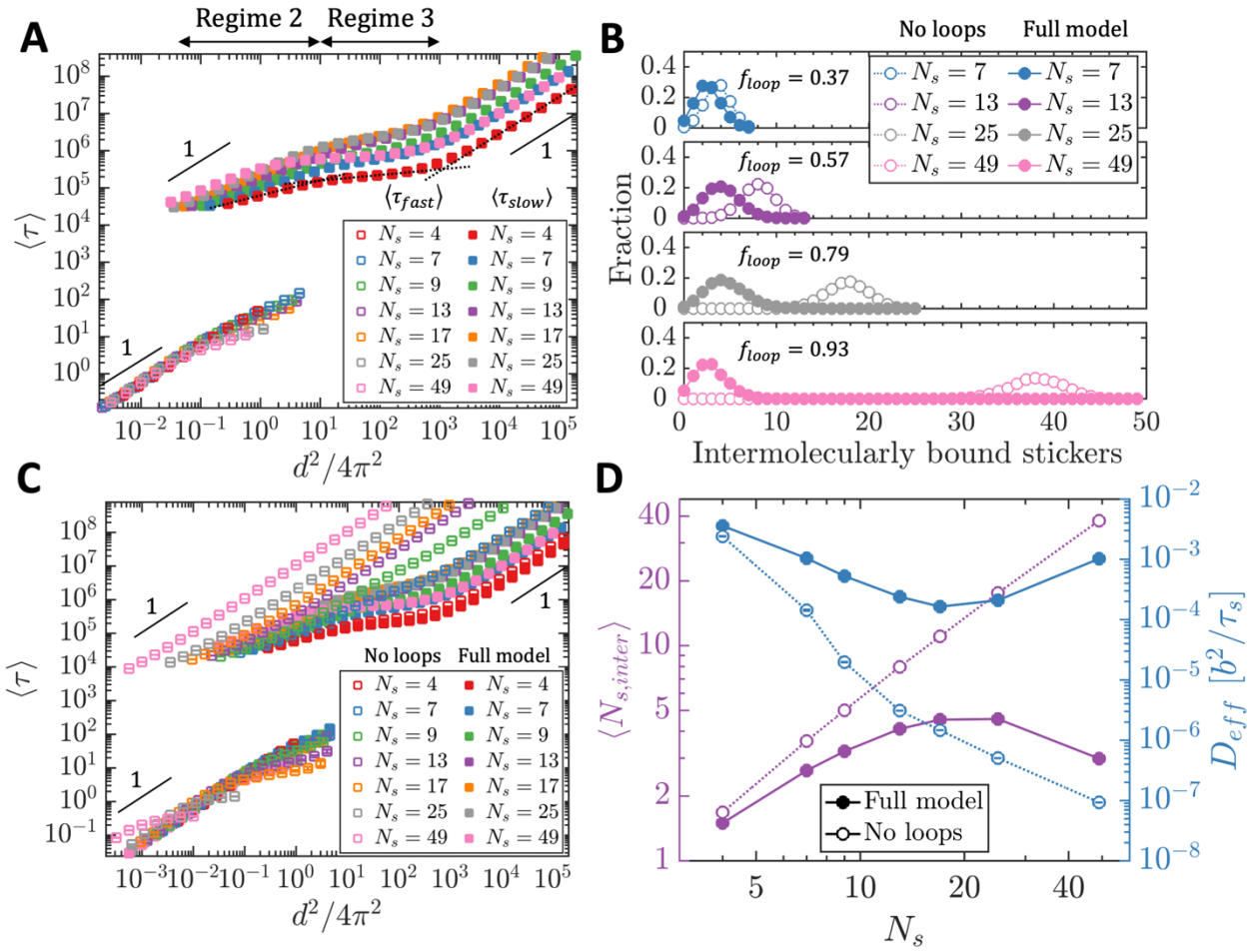

Figure 6. (A) Effect of number of stickers per chain on the characteristic time constants as a function of the square length scale $d^2/4\pi^2$, from simulations with $\phi = 1$, $K_{eq} = 15$, and $k_A = 0.0002$. (B) Histograms of the average number of intermolecularly bound stickers per chain for different values of N_s, both in the full model and in the loop-free model. Loop fractions for the full model are listed. (C) Comparison of chain diffusion for various values of N_s in the full model and in a loop-free model where intramolecular reactions are disabled. (D) Average number of intermolecularly bound stickers, $\langle N_{s,inter}\rangle$, and long-time effective diffusion coefficient, D_{eff}, as a function of N_s.

hypothesis, Figure 6a shows the chain diffusive behavior at different values of N_s with constant chain length ($N = 49$ beads) and volume fraction ($\phi = 1$). The diffusion profiles exhibit the same qualitative regimes as in the 4-sticker case, including short-time Fickian scaling for the fast mode and two regimes of apparent superdiffusion for the slow mode before terminal Fickian scaling. The short-time values of τ_{fast} are equal to within error for all sticker densities, suggesting that segmental chain motion on length scales smaller than the sticker spacing is unaffected by binding. However, the size of the cage (determined as length scale at which the slow mode appears)

decreases with N_s, consistent with the reduction in the mean-square extension of the strands between stickers $\Delta N_{strand} b^2$ at constant chain length (see Fig. S14).

The behavior of the slow relaxation time τ_{slow} shows a strong dependence on N_s, including a crossover between the short- and long-d^2 regimes (Regimes 2 through 4) for $N_s > 17$. This indicates that while the diffusion coefficient immediately following exit from the cage decreases monotonically with N_s, the terminal diffusivity in the long-time Fickian regime follows a non-monotonic dependence on N_s (see Fig. 6d). Notably, both regimes of superdiffusive scaling (Regimes 2 and 3) are present for all values of N_s, with the curves showing no sign of transitioning to the purely Fickian scaling at high sticker density predicted by mean-field theories.[24,28] These results are consistent with self-diffusion experiments of metal-coordinate polymers[29] and suggest that hopping is an important diffusive mode even when the number of stickers per chain is increased to 49 at constant chain concentration.

The ability for high-sticker-density chains to hop can be explained by their enhanced propensity to form intramolecular loops, which reduces the number of stickers required to unbind from the network to begin a hopping step. The loop fraction in the system is determined by the balance between intermolecular and intramolecular binding rates, which are governed by the global and local (i.e., within the pervaded volume of a chain) sticker concentrations. As shown in Figs. 6b and S16, increasing N_s at constant chain length and concentration results in a monotonic increase in the loop fraction, from 19% for the 4-sticker chains to 93% for the 49-sticker chains. The increase in loop fraction with N_s occurs due to both the smaller volume of the strands between stickers and the greater number of sticker combinations that can intramolecularly react, as also shown in recent MD simulations studying the static properties of associative polymer melts.[53] This higher loop fraction counteracts the increase in N_s by decreasing the number of stickers per chain

that are intermolecularly bound, as shown by the histograms in Fig. 6b. The average number of intermolecularly bound stickers per chain, $\langle N_{s,inter} \rangle$, increases with sticker density up to $N_s = 17$ before decreasing at higher N_s, where the enhancement of looping reactions begins to outweigh the increase in total number of stickers per chain. This reduction in $\langle N_{s,inter} \rangle$ in turn enhances the likelihood of chain hopping, resulting in the crossover of the diffusion curves seen in Fig. 6a.

The role of loops in enabling superdiffusive scaling at high sticker density is clearly seen by comparing the simulation results between the full model and a loop-free model in which intramolecular reactions are explicitly disabled (Fig. 6c). In contrast to the full model, the diffusion curves in the loop-free model shift monotonically to higher values of τ with N_s, which is accompanied by a decrease in the width of the superdiffusive scaling regimes. Figure 6d shows the effect of increasing N_s on the long-time effective diffusion coefficient D_{eff}. In the full model, the presence of loops results in an increase in D_{eff} for $N_s > 17$, whereas in the loop-free model there is a monotonic decrease in D_{eff} with N_s. These results explain the origin of the experimental observations of superdiffusive scaling at high sticker density,[29] demonstrating the enhancement in loops that allows hopping to remain a significant diffusive mode even with a large number of stickers per chain (at constant chain concentration). It is important to note that in the simulations, the binding equilibrium constant K_{eq} is kept constant for each sticker regardless of the number of bound stickers or total number of stickers on a chain. Recent studies by Rapp *et al*[35,36] have suggested that structural inhomogeneities and geometric constraints in real associative gels may reduce the effective binding strength with increasing sticker density due to the loss of conformational entropy associated with strand tethering. Although these effects are not accounted for in the mean-field description of sticker binding used here, the simulations show that chains can hop at high N_s even without an entropic pentalty for binding. Rather, the enhancement in the

looping propensity with increasing N_s is sufficient to allow hopping, even with the strength of each bond kept constant. However, these results do not contraindicate the entropic effect on K_{eq}, which may indeed be present in experimental systems. As suggested by Rapp *et al*, the effect of conformational entropy on the looping vs. bridging propensities is expected to increase the looping probability at high N_s and enhance the contribution of hopping even further compared to the mean-field description. Further study is required to probe the effect of chain conformation on sticker binding energy, which is treated as a pre-defined parameter in this work.

Distribution of hopping events. The effect of sticker density (N_s) on the contribution of the hopping mode can be further elucidated by examining the duration and displacement of hopping events in the system at different values of N_s. Figure 7a presents the probability distribution of the time duration that a molecule spends hopping before rebinding to the network, $p(\tau_{hop})$, for each value of N_s from simulations with $K_{eq} = 15$, $k_A = 0.0002$, and $\phi = 1$. For all sticker densities, the hopping duration τ_{hop} follows an exponential distribution (solid curves), which arises from the Poisson nature of the sticker binding process,[45]

$$p(\tau_{hop}) = \frac{1}{\langle \tau_{hop} \rangle} \exp\left(-\frac{\tau_{hop}}{\langle \tau_{hop} \rangle}\right) \tag{8}$$

where $\langle \tau_{hop} \rangle$ is the mean hopping duration. A non-monotonic dependence of $\langle \tau_{hop} \rangle$ with N_s is observed, as shown in Fig. 7c. The initial decrease in $\langle \tau_{hop} \rangle$ with N_s can be explained by the increase in the number of free stickers on the chain, which increases the rate of rebinding to the network. However, for $N_s > 17$, the increase in number of stickers per chain is compensated for (and eventually outweighed) by the increase in the loop fraction, which decreases the number of free stickers in the system, such that that the hopping duration begins to increase with sticker density at high N_s.

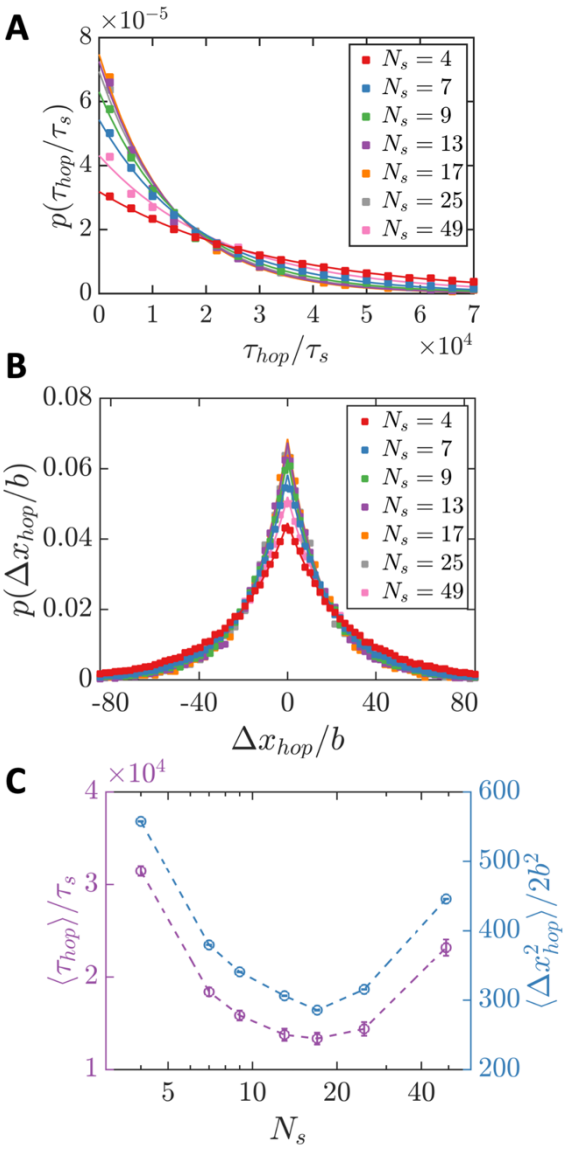

Figure 7. (A) Distribution of the hopping duration, τ_{hop}, for varying N_s. Solid curves are fits to exponential distributions given by Eq. 8. (B) Distribution of 1D hopping displacement for the same simulations as in panel A. Solid lines are analytical predictions for the displacement distribution given by Eq. 9, using the mean hopping duration $\langle \tau_{hop} \rangle$ obtained from the data in panel A. (C) Mean hopping duration $\langle \tau_{hop} \rangle$ and mean-square 1D hopping displacement $\langle \Delta x_{hop}^2 \rangle / 2$ as a function of N_s obtained from the distributions shown in panels A and B, demonstrating a non-monotonic dependence on N_s. Error bars are uncertainties based on the histogram bin sizes.

Figure 7b presents the normalized distribution of the 1D hopping displacement, averaged over three dimensions, for each value of N_s. The hopping displacement distribution, $p(\Delta x_{hop})$, can be predicted from the hopping duration distribution, $p(\tau_{hop})$, and the displacement density of each hopping event of duration τ_{hop}:

$$p(\Delta x_{hop}) = \int_0^\infty p(\tau_{hop}) p(\Delta x_{hop}; \tau_{hop}) d\tau_{hop} \tag{9}$$

where the displacement of a hop with duration τ_{hop} follows a Gaussian distribution:

$$p(\Delta x_{hop}; \tau_{hop}) = \frac{1}{\sqrt{4\pi D_{free} \tau_{hop}}} \exp\left(-\frac{\Delta x_{hop}^2}{4 D_{free} \tau_{hop}}\right) \tag{10}$$

with the diffusivity of a hopping chain D_{free} given by Einstein's relation:

$$D_{free} = \frac{k_B T}{N\xi} \tag{11}$$

As shown by the solid lines in Fig. 7b, the hopping displacement distributions in the simulations are well-captured by the prediction of Eq. 9, using the values of $\langle \tau_{hop} \rangle$ calculated from the data in Fig. 7a. Consistent with $\langle \tau_{hop} \rangle$, the mean-square hopping displacement $\langle \Delta x_{hop}^2 \rangle$ also displays a non-monotonic dependence on N_s (Fig. 7c) due to changes in the loop fraction as described.

On long length and time scales, the occurrence of multiple hopping events is expected to result in terminal Fickian diffusion with an effective diffusivity governed by the characteristic hopping frequency and displacement.[30,37] Figure 7c plots the mean hopping duration, $\langle \tau_{hop} \rangle$, along with the characteristic 1D mean-square displacement of a single hop, $d_{hop}^2/4\pi^2 = \langle \Delta x_{hop}^2 \rangle/2$. A comparison between the $\langle \Delta x_{hop}^2 \rangle/2$ values and the diffusion curves shown in Fig. 6a indicates that the characteristic hopping displacements of $300b^2 < \langle \Delta x_{hop}^2 \rangle/2 < 600b^2$ align with the transition from superdiffusive scaling to terminal Fickian scaling (Regime 3 to Regime 4). On this length scale, chains begin to undergo multiple hopping events, leading to terminal Fickian diffusion governed by the hopping diffusivity. Notably, these results suggest a link between transitions in the $\langle \tau \rangle$ vs d^2 curve, which is accessible by ensemble-averaged scattering measurements,[29,30,33,34] and the characteristic length scale of molecular hopping events. Examining

recent forced Rayleigh scattering diffusion measurements of metal-coordinate polymer gels[29] in this context suggests an average hopping displacement in these systems on the order of $1-10$ μm, several orders of magnitude larger than the chain radius of gyration. However, it is important to note that a direct experimental observation of chain hopping has yet to be performed.[29,33,34]

Effect of chain concentration. The loop fraction in the system and the resulting dynamics are governed by the balance between the local and global sticker densities, which depend respectively on the number of stickers per chain (N_s) and the chain concentration (ϕ). At low ϕ and high N_s, interchain interactions are minimal, promoting loop formation. However, at large ϕ different chains interpenetrate and intermolecular association becomes likely. As seen in Fig. 8, increasing ϕ for each value of N_s reduces the width of the upper superdiffusive regime caused by hopping. The suppression in superdiffusive scaling arises primarily due to the decrease in the loop fraction in favor of intermolecular bonds at higher concentration (Fig. S16), which decreases the equilibrium fraction of chains detached from the network. As N_s increases, the diffusive behavior of a chain with loops switched off at $\phi = 1$ (open symbols in Fig. 8) becomes qualitatively similar to that of a chain with loops enabled at significantly higher concentration (e.g., $\phi = 10$).

When both N_s and ϕ are high, the global sticker density in the system ($\sim N_s\phi$) is maximal, and dynamics approach the mean-field limit of Fickian center-of-mass chain diffusion on all length scales larger than the cage size as predicted by the sticky Rouse model.[24,25,28] As seen in Fig. 8d, when $N_s = 49$ and $\phi = 10$, Fickian scaling is observed for almost all length scales beyond the caging regime. This likely arises from (1) the suppression of hopping due to the decrease in the loop fraction at high ϕ and (2) the convergence of the walking diffusive states at high N_s (Fig. 5), suppressing the extent of superdiffusive scaling in both Regimes 2 and 3. The results show that mean-field dynamics of purely Fickian diffusion can be achieved when both N_s and ϕ are large.[24,28]

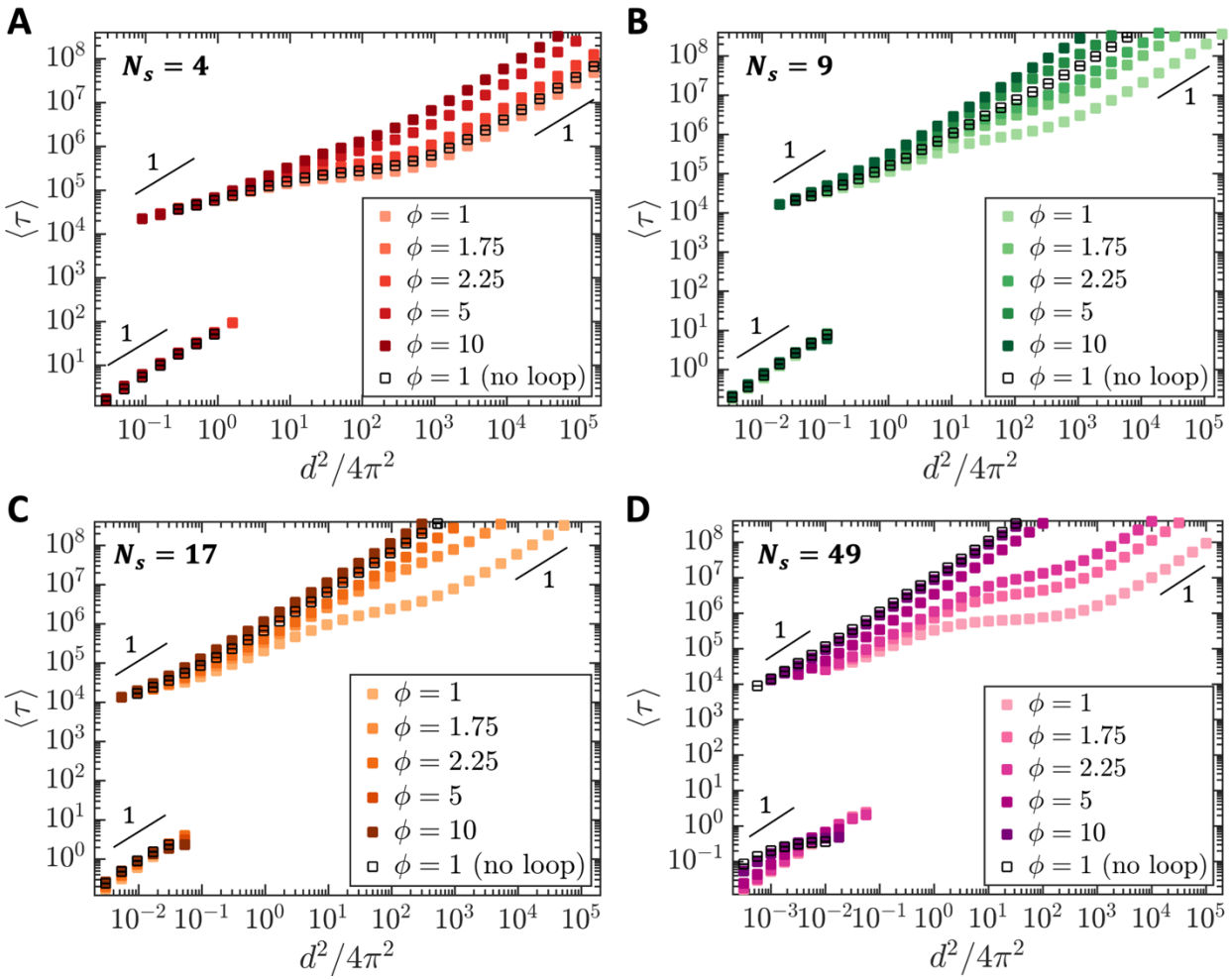

Figure 8. Effect of chain concentration ϕ on diffusion for sticker densities of (A) $N_s = 4$, (B) $N_s = 9$, (C) $N_s = 17$, and (D) $N_s = 49$ per chain. Simulation parameters were $k_A = 0.0002$, $K_{eq} = 15$, and $\phi = 1$. Open black symbols show the diffusive behavior of chains at $\phi = 1$ in the loop-free model for comparison.

This regime of both high concentration and high sticker density results in long diffusion times and was not accessed in recent studies of metal-coordinate linear polymers due to limitations in the range of forced Rayleigh scattering.[29] In addition, these high concentrations ($\phi \geq 10$) may be above the entanglement threshold in real associative networks,[29] which may result in qualitative changes to chain diffusive mechanisms on different length scales.[54,55] For unentangled gels, systems with faster sticker kinetics but otherwise identical parameters may enable diffusion

measurements at this mean-field limit of Fickian diffusion on all length scales, but such studies have not been performed to date.[29,33,36]

At low $d^2/4\pi^2$, the values of τ_{slow} in each panel of Fig. 8 converge to a single point, signifying an intrinsic, concentration-independent dissociation time corresponding to the exit from the cage. Longer timescales involve multiple sticker association and dissociation events, allowing the coexistence of dynamic modes and a concentration-dependent diffusivity. However, it is important to note that the single-spring length and relaxation time used as the units of length and time in the simulation are functions of concentration due its effect on the correlation blob size.[43] The blob size (equal to the single-spring length b in the simulation) decreases with concentration and its relaxation time τ_s increases, as governed by solvent quality.[43,51] When transformed to real units, the diffusion curves in Fig. 8 show the same qualitative trends but are more spread out in space than when plotted with the scaled units; see Fig. S12.

Effect of sticker kinetics and equilibrium constant. While the sticker density in the system affects the extent of superdiffusive scaling largely through changes in the intermolecular and intramolecular bond fractions, the contribution of the hopping mode can be more directly controlled through the sticker equilibrium constant (K_{eq}) and kinetic rate constants (k_A and k_D). Figure 9 compares the effects of independently varying K_{eq} and k_D from simulations with $N_s = 4$ and $\phi = 1$. As seen in Fig. 9a, increasing K_{eq} slows diffusion on long length scales due to the greater equilibrium fraction of bound stickers, which reduces the frequency and duration of hopping events. However, varying K_{eq} has minimal effect on the timescale of exit from the cage, which is governed by $\tau_{exit} = k_D^{-1}/2$ and independent of the hopping mode. In contrast, increasing the association/dissociation rate constants at constant K_{eq} (equivalent to decreasing k_D^{-1}) reduces the diffusion timescale on small length scales, immediately after a chain exits the cage, but has

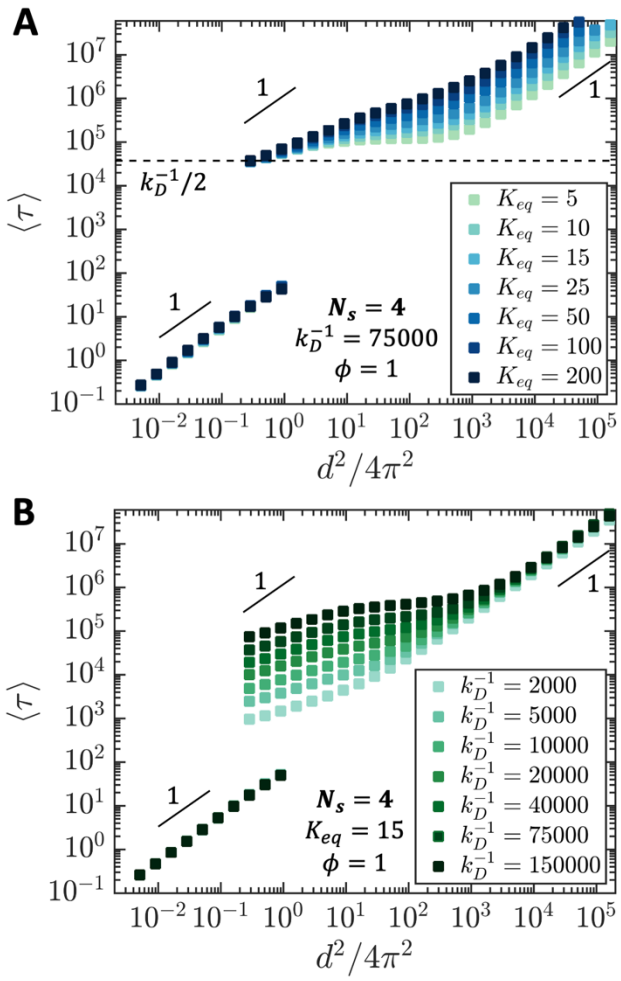

Figure 9. (a) Effect of varying K_{eq} at constant $k_D^{-1} = 75000$ on chain diffusion behavior for a system with $N_s = 4$ and $\phi = 1$. (b) Effect of varying k_D at constant $K_{eq} = 15$ for the same system.

minimal effect on the long-time diffusivity (Fig. 9b). This can be rationalized by recognizing that at constant K_{eq}, changes in the sticker binding kinetics concomitantly affect both the frequencies of beginning and ending a hopping event. That is, the enhancement in the hopping frequency when k_D is increased is matched by the greater rate of rebinding due to the increase in k_A (note that $K_{eq} = k_A/k_D$). This results in the average fraction of molecules undergoing a hopping step being a function of K_{eq} only, independent of k_D (Fig. S17). Because the long-time diffusivity is governed largely by the number of hopping molecules in the system (see Fig. 10), the curves converge on long timescales to a constant terminal diffusivity for all values of k_D. Thus, the results in Fig. 9

demonstrate that the extent of superdiffusive scaling can be tuned by varying both the equilibrium constant and the kinetics, but through opposite effects on the chain diffusion rate at either end of the length scale range.

Analytical prediction of the walking and hopping diffusivities. Analytical expressions for the hopping and walking diffusivities in the system can be formulated by considering the relevant dynamic processes underlying each mechanism. The hopping diffusivity can be estimated as the diffusivity of a free chain, $D_{free} = k_B T/N\xi$, multiplied by the average fraction of hopping chains in the system, p_0:

$$D_{hop} = p_0 \left(\frac{k_B T}{N\xi}\right) \tag{12}$$

Using the arguments developed in the sticky Rouse theory,[24] a scaling prediction for the walking diffusivity can be obtained from the radius of gyration and terminal relaxation time of a chain:

$$D_{walk,sc} \approx \frac{R_g^2}{\tau_{chain}} = \frac{Nb^2/6}{\langle N_{inter}\rangle^2 (k_D^{-1}/2)} \tag{13}$$

where τ_{chain} is the chain's longest relaxation time, which is proportional to the sticker lifetime, and $\langle N_{inter}\rangle$ is the average number of stickers per chain that are intermolecularly bound to the network. In addition to the scaling theory, a more rigorous analytical prediction for the walking diffusivity ($D_{walk,an}$) can be obtained by calculating the expected mean-square center-of-mass displacement of each chain in the system during a walking step (i.e., after unbinding a sticker), using its specific sticker bonding configuration. As shown earlier in Eq. 7, the walking diffusivity for a kinetics-limited system can be written in terms of the mean-square center-of-mass displacement during the walking step and the timescale for sticker dissociation:

$$D_{walk,an} \approx 2k_D \sum_{s=2}^{N_s} p_s \frac{\langle \Delta R_{CM,(s-1)}^2 \rangle}{6} \tag{14}$$

where $2k_D$ is the sticker unbinding frequency, p_s is the probability of having s stickers bound to the network, and $\langle \Delta R^2_{CM,(s-1)} \rangle$ is the mean-square center-of-mass displacement of a chain after unbinding a sticker, averaged over all possible unbinding events. The mean-square displacement after each possible unbinding event, $\langle \Delta R^2_{CM,(s-1)} \rangle$, can be analytically calculated from the configurational partition function of a Gaussian chain at fixed sticker bonding,[56–58] assuming that the original position of the recently detached sticker follows a Gaussian distribution within the pervaded volume of the strand and that strands relax to their equilibrium conformational distribution during the time the sticker is detached.[39,42] A full derivation for this approach of calculating $\langle \Delta R^2_{CM,(s-1)} \rangle$ given a chain's particular sticker bonding configuration is provided in Section IV of the Supporting Information. Importantly, this analytical approach allows the exact topological structure of each chain, including loops, to be captured in the estimate for $D_{walk,an}$.

As seen in Fig. 10, the analytical predictions for the walking and hopping diffusivities (Eqs. 12 and 14) show good qualitative agreement with the results from simulation in both the full and no-hopping models, capturing both the non-monotonic trend in the hopping diffusivity (due to changes in the loop fraction; see Fig. 6) and the monotonic decrease in the walking diffusivity with increasing N_s. The scaling prediction $D_{walk,sc}$ given in Eq. 13 also provides a reasonable prediction for the walking diffusivity, though it becomes less accurate at high N_s due to its neglect of the specific bonding configuration of each chain, particularly the increased loop fraction. Overall, the analytical predictions provide insight into the link between the static topological structure of the network, bond lifetime, and the relative importance of each diffusive mechanism on various length scales, with good agreement with the trends seen in simulation.

Comparison to experiment. A comparison of the simulations to recent experiments on associative linear polymer gels of different types[29,33] suggests that this molecular model can

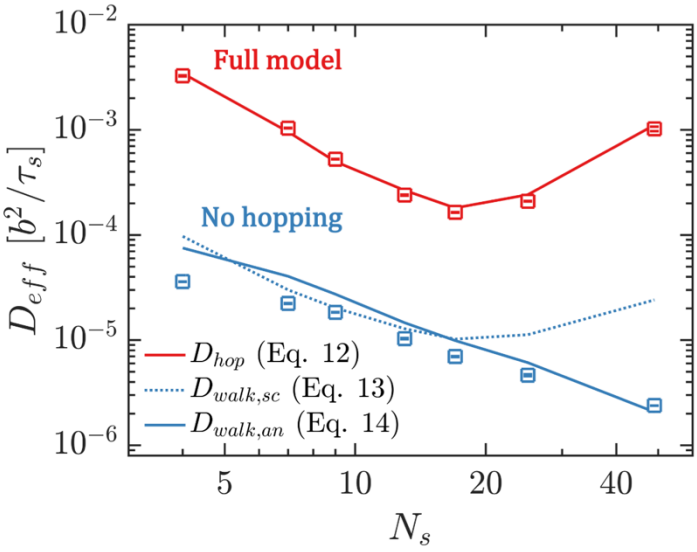

Figure 10. Comparison of the simulation results (symbols) for the full and hopping-free models with analytical and scaling predictions (lines) for the walking and hopping diffusivities, D_{walk} and D_{hop}, obtained using Eqs. 12-14. The simulation parameters are $\phi = 1, k_A = 0.0002$, and $K_{eq} = 15$.

capture key dynamics in associative systems across a range of length scales. Figure 11a compares the simulation results with self-diffusion measurements of unentangled gels composed of linear coiled-coil proteins with 4 stickers per chain.[33] Dynamics of the coiled-coil proteins were measured using neutron spin-echo spectroscopy and forced Rayleigh scattering, accessing a wide range of length scales; the units have been scaled by the junction spacing and Zimm time of the strands to allow comparison with the simulations (see Ref. [33] for experimental details). As seen in Figs. 11a and 11b, the simulation results for $N_s = 4$ at different ϕ show qualitative agreement with the experimental results for the protein gels, including the caging regime and the two regimes of superdiffusive scaling before terminal Fickian diffusion. The simulations provide a well-defined molecular basis for each regime, showing explicit transitions from caging to walking and subsequently hopping as the origin for the two superdiffusive regimes in the protein gels. The simulations demonstrate the narrowing of the upper superdiffusive regime with concentration seen experimentally (Fig. 11b) to result from an enhancement in intermolecular binding, which decreases the fraction of hopping molecules. However, in the protein gels, the scaled relaxation

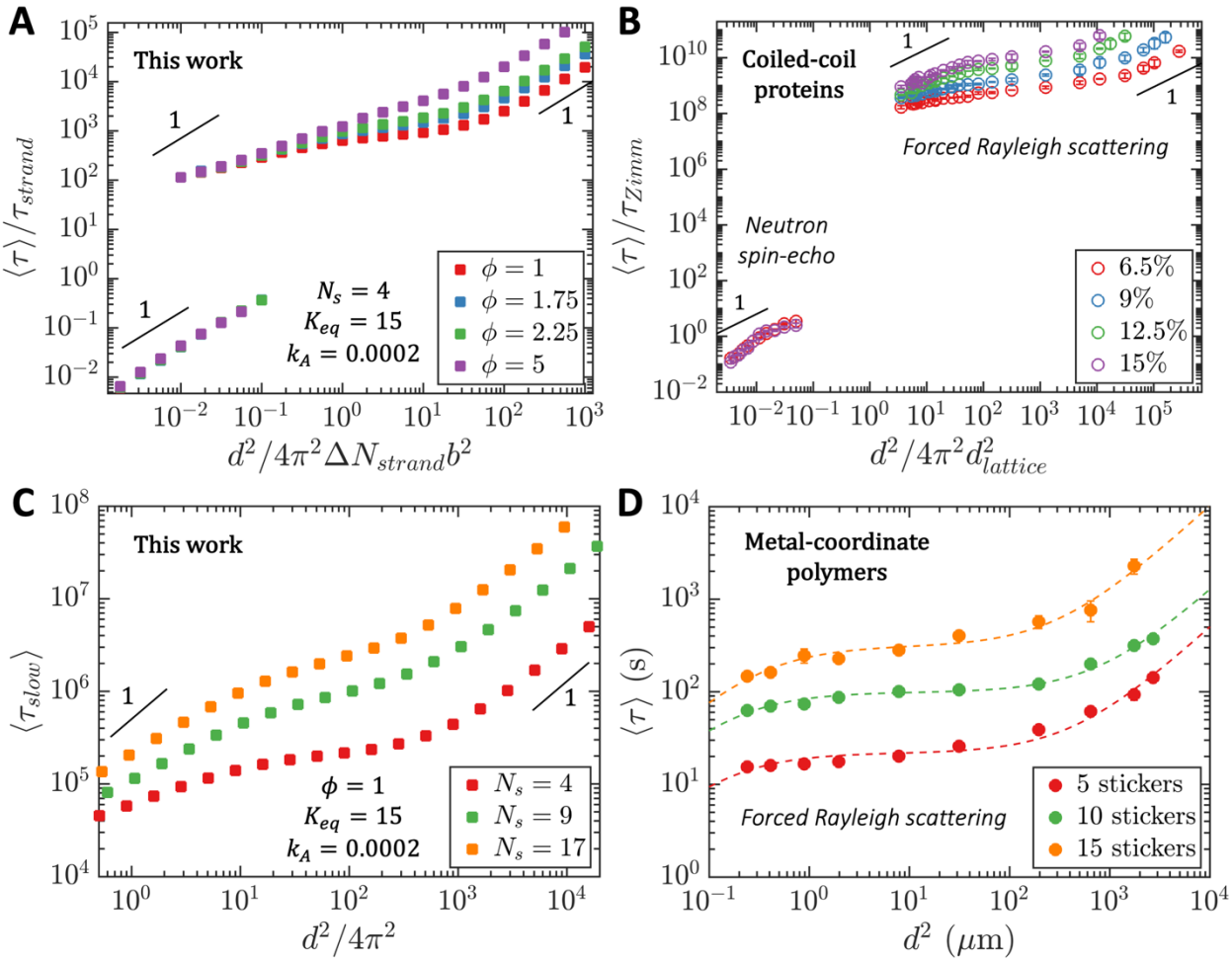

Figure 11. (A) Simulation results for $N_s = 4$ at various concentrations (the same data as in Fig. 8a). (B) Experimental self-diffusion measurements of 4-sticker coiled-coil protein hydrogels of various concentrations obtained using neutron spin-echo spectroscopy and forced Rayleigh scattering. Data are obtained from Ref. 31. (C) Simulation results for the slow relaxation mode, τ_{slow}, for various values of N_s at $\phi = 1$ (the same data as in Fig. 6a). (D) Self-diffusion measurements of associative poly(dimethylacrylamide) gels based on Ni^{2+}-histidine coordination bonds with different numbers of stickers per chain obtained using forced Rayleigh scattering. Data are obtained from Ref. 27. The dashed lines are fits to a two-state model as described in Ref. 27 and are presented as a guide to the eye.

times in the superdiffusive and terminal Fickian regimes are ~6 orders of magnitude greater than those in the simulations. This is largely a consequence of differences in association/dissociation kinetics of the associative bonds in the protein gels ($\tau_D/\tau_{Zimm} \approx 10^7 - 10^8$; see Ref.[33]) compared to those in the simulations ($k_D^{-1}/\tau_{strand} = 293$), which determine the characteristic timescales of self-diffusion. In addition, the scaling of the terminal diffusivity with concentration in the protein

gels ($D_{eff} \sim \phi^{-6.1 \pm 0.5}$; Ref.[33]) is stronger than that observed in simulation (in real units, $D_{eff} \sim \phi^{-1.9 \pm 0.2}$; Fig. S13). This discrepancy may arise from differences in the sticker functionality between the simulations (binary association) and the protein hydrogels (pentameric association), as well as contributions from trapped entanglements or multi-chain clustering in the protein gels that are not accounted for in the simulations; such network inhomogeneities or topological entrapments may enhance the slowing of chain dynamics with concentration to a greater extent than that due to binding site density alone.[24] However, further study is required to fully elucidate the role of such multi-chain effects on self-diffusion in the gel.

As a further comparison to a chemically distinct system, Fig. 11d shows self-diffusion measurements of Ni^{2+}-coordinated poly(dimethylacrylamide) chains of various sticker densities using forced Rayleigh scattering.[29] The experimental results show a similar extent of superdiffusive behavior for all sticker densities probed, both in the width and scaling exponent of the upper superdiffusive regime, between 5 and 15 stickers per chain. The simulations (Fig. 11c) capture this qualitative behavior and establish the key role of loops in enabling apparent superdiffusion at higher sticker density. Thus, despite the approximations inherent to the coarse-grained approach used here, the simulations are able to qualitatively capture all of the diffusive regimes observed experimentally, revealing insight into the origins of chain diffusive behavior in multiple distinct systems.

4. CONCLUSIONS

This work develops a generalized Brownian dynamics model of gel-forming linear polymers with pendant stickers, exploring the effect of varying the sticker density, chain concentration, and binding kinetics on their dynamics across a range of length scales. The simulations are able to deconvolute the diffusive modes of hopping and walking, demonstrating

clear transitions from caging to walking and subsequently to hopping as the origin for two regimes of superdiffusive scaling on mesoscopic length scales before terminal Fickian diffusion. Notably, the simulations show that the lower superdiffusive regime occurs even in the absence of hopping, which is attributed to the increase in the average strand pervaded volume upon sticker detachment during the transition from caging to walking. The presence of multiple dynamic modes results in a non-Gaussian real-space displacement distribution on timescales that correlate with the presence of superdiffusive scaling. Disabling hopping is found to suppress, but not eliminate, the non-Gaussian behavior in the real-space distribution, which is attributed to the presence of superdiffusive behavior by walking alone. In addition, the mean-square displacement of hopping events is computed for each sticker density, which is found to correspond with the transition length scale from apparent superdiffusion to terminal Fickian diffusion primarily dictated by the hopping mode.

The simulations also demonstrate that the extent of superdiffusion by hopping is highly sensitive to the sticker binding kinetics, equilibrium constant, and total chain concentration. When the number of stickers per chain is increased at constant concentration, the enhanced prevalence of loops counteracts the greater sticker density in the system, resulting in a non-monotonic trend of the terminal diffusivity and enabling hopping of chains with as many as 49 stickers. When both the chain concentration and the sticker density per chain are increased, dynamics approach the mean-field limit of Fickian diffusive scaling on all length scales. Analytical predictions are developed to estimate the walking and hopping diffusivities, finding qualitative agreement with simulation and revealing the link between the static network topology and contribution of each self-diffusive mode. Finally, a comparison with recent diffusion measurements of analogous associative polymer gels finds qualitative agreement, suggesting that this coarse-grained model

can capture key dynamic trends in chemically distinct systems. It is anticipated that this model can be generalized to other associative polymer systems, including those with different chain architectures and sticker distributions along the chain, and can provide insight into the design of soft materials for various applications from biomedicine to self-healing materials.

SUPPORTING INFORMATION: Model validation, simulation equilibration, mean-square displacement over time, chain diffusion curves in real units, and other supplementary figures.

ACKNOWLEDGEMENTS

This work was supported by the National Science Foundation (Award DMR-1709315). A.R. acknowledges support from the Department of Defense through a National Defense Science and Engineering Graduate Fellowship. Simulations were run in part using the Extreme Science and Engineering Discovery Environment (XSEDE), which is supported by the National Science Foundation (Award ACI-1548562). The authors thank T.-S. Lin and A. Arora for helpful discussions.

REFERENCES

(1) Stuart, M. A. C.; Huck, W. T. S.; Genzer, J.; Müller, M.; Ober, C.; Stamm, M.; Sukhorukov, G. B.; Szleifer, I.; Tsukruk, V. V.; Urban, M.; et al. Emerging Applications of Stimuli-Responsive Polymer Materials. *Nat. Mater.* **2010**, *9* (2), 101–113.

(2) Webber, M. J.; Appel, E. A.; Meijer, E. W.; Langer, R. Supramolecular Biomaterials. *Nat. Mater.* **2015**, *15* (1), 13–26.

(3) Lopez, J.; Mackanic, D. G.; Cui, Y.; Bao, Z. Designing Polymers for Advanced Battery Chemistries. *Nat. Rev. Mater.* **2019**, *4* (5), 312–330.

(4) Feldman, K. E.; Kade, M. J.; Meijer, E. W.; Hawker, C. J.; Kramer, E. J. Model Transient Networks from Strongly Hydrogen-Bonded Polymers. *Macromolecules* **2009**, *42* (22), 9072–9081.

(5) Yount, W. C.; Loveless, D. M.; Craig, S. L. Small-Molecule Dynamics and Mechanisms Underlying the Macroscopic Mechanical Properties of Coordinatively Cross-Linked Polymer Networks. *J. Am. Chem. Soc.* **2005**, *127* (41), 14488–14496.

(6) Castelletto, V.; Hamley, I. W.; Yuan, X. F.; Kelarakis, A.; Booth, C. Structure and Rheology of Aqueous Micellar Solutions and Gels Formed from an Associative Poly(Oxybutylene)-Poly(Oxyethylene)-Poly(Oxybutylene) Triblock Copolymer. *Soft Matter* **2005**, *1* (2), 138–145.

(7) Tang, S.; Olsen, B. D. Relaxation Processes in Supramolecular Metallogels Based on Histidine-Nickel Coordination Bonds. *Macromolecules* **2016**, *49* (23), 9163–9175.

(8) Shen, W.; Kornfield, J. A.; Tirrell, D. A. Dynamic Properties of Artificial Protein Hydrogels Assembled through Aggregation of Leucine Zipper Peptide Domains. *Macromolecules* **2007**, *40* (3), 689–692.

(9) Seiffert, S.; Sprakel, J. Physical Chemistry of Supramolecular Polymer Networks. *Chem. Soc. Rev.* **2012**, *41* (2), 909–930.

(10) Craig, S. L.; Xu, D. Physical Organic Chemistry of Supramolecular Polymers. *Langmuir* **2007**, *23*, 1626–1634.

(11) Frey, S.; Richter, R. P.; Görlich, D. FG-Rich Repeats of Nuclear Pore Proteins Form a Three-Dimensional Meshwork with Hydrogel-like Properties. *Science* **2006**, *314* (5800), 815–817.

(12) Kim, M.; Chen, W. G.; Kang, J. W.; Glassman, M. J.; Ribbeck, K.; Olsen, B. D. Artificially Engineered Protein Hydrogels Adapted from the Nucleoporin Nsp1 for Selective Biomolecular Transport. *Adv. Mater.* **2015**, *27* (28), 4207–4212.

(13) Yang, Y. J.; Mai, D. J.; Dursch, T. J.; Olsen, B. D. Nucleopore-Inspired Polymer Hydrogels for Selective Biomolecular Transport. *Biomacromolecules*. 2018, pp 3905–3916.

(14) van der Heijden, T.; Modesti, M.; Hage, S.; Kanaar, R.; Wyman, C.; Dekker, C. Homologous Recombination in Real Time: DNA Strand Exchange by RecA. *Mol. Cell* **2008**, *30* (4), 530–538.

(15) Yan, X.; Wang, F.; Zheng, B.; Huang, F. Stimuli-Responsive Supramolecular Polymeric Materials. *Chem. Soc. Rev.* **2012**, *41* (18), 6042–6065.

(16) Yang, Y.; Urban, M. W. Self-Healing Polymeric Materials. *Chem. Soc. Rev.* **2013**, *42* (17), 7446–7467.

(17) Olsen, B. D.; Kornfield, J. A.; Tirrell, D. A. Yielding Behavior in Injectable Hydrogels from Telechelic Proteins. *Macromolecules* **2010**, *43* (21), 9094–9099.

(18) Shen, W.; Zhang, K.; Kornfield, J. A.; Tirrell, D. A. Tuning the Erosion Rate of Artificial Protein Hydrogels through Control of Network Topology. *Nat. Mater.* **2006**, *5* (2), 153–158.

(19) Li, C. H.; Wang, C.; Keplinger, C.; Zuo, J. L.; Jin, L.; Sun, Y.; Zheng, P.; Cao, Y.; Lissel, F.; Linder, C.; et al. A Highly Stretchable Autonomous Self-Healing Elastomer. *Nat. Chem.* **2016**, *8* (6), 618–624.

(20) Holten-Andersen, N.; Harrington, M. J.; Birkedal, H.; Lee, B. P.; Messersmith, P. B.; Lee, K. Y. C.; Waite, J. H. PH-Induced Metal-Ligand Cross-Links Inspired by Mussel Yield Self-Healing Polymer Networks with near-Covalent Elastic Moduli. *Proc. Natl. Acad. Sci.* **2011**, *108* (7), 2651–2655.

(21) Olivia R. Cromwell, J. C.; Guan, and Z. Malleable and Self-Healing Covalent Polymer Networks through Tunable Dynamic Boronic Ester Bonds. *J Am Chem Soc* **2009**, *48* (1), 35–56.

(22) Annable, T.; Buscall, R.; Ettelaie, R.; Whittlestone, D. The Rheology of Solutions of Associating Polymers: Comparison of Experimental Behavior with Transient Network Theory. *J. Rheol. (N. Y. N. Y).* **1993**, *37* (4), 695–726.

(23) Tanaka, F.; Edwards, S. F. Viscoelastic Properties of Physically Cross-Linked Networks. Transient Network Theory. *Macromolecules* **1992**, *25* (5), 1516–1523.

(24) Rubinstein, M.; Semenov, A. N. Thermoreversible Gelation in Solutions of Associative Polymers. 2. Linear Dynamics. *Macromolecules*. Macromolecules 1998, pp 1386–1397.

(25) Semenov, A. N.; Rubinstein, M. Thermoreversible Gelation in Solutions of Associative Polymers. 1. Statics. *Macromolecules* **1998**, *31*, 1373–1385.

(26) Green, M. S.; Tobolsky, A. V. A New Approach to the Theory of Relaxing Polymeric Media. **1946**, *455* (1943), 80–92.

(27) Tripathi, A.; Tam, K. C.; McKinley, G. H. Rheology and Dynamics of Associative Polymers in Shear and Extension: Theory and Experiments. *Macromolecules* **2006**, *39* (5), 1981–1999.

(28) Baxandall, L. G. Dynamics of Reversibly Cross-Linked Chains. *Macromolecules* **1989**, *22*, 1982–1988.

(29) Mahmad Rasid, I.; Holten-Andersen, N.; Olsen, B. D. Anomalous Diffusion in Associative Networks of High-Sticker-Density Polymers. *Macromolecules* **2021**, *54*, 1354–1365.

(30) Tang, S.; Wang, M.; Olsen, B. D. Anomalous Self-Diffusion and Sticky Rouse Dynamics in Associative Protein Hydrogels. *J. Am. Chem. Soc.* **2015**, *137* (11), 3946–3957.

(31) Hackelbusch, S.; Rossow, T.; Van Assenbergh, P.; Seiffert, S. Chain Dynamics in Supramolecular Polymer Networks. *Macromolecules*. 2013, pp 6273–6286.

(32) Chen, Q.; Tudryn, G. J.; Colby, R. H. Ionomer Dynamics and the Sticky Rouse Model. *J. Rheol. (N. Y. N. Y).* **2013**, *57* (5), 1441–1462.

(33) Rao, A.; Yao, H.; Olsen, B. D. Bridging Dynamic Regimes of Segmental Relaxation and Center-of-Mass Diffusion in Associative Protein Hydrogels. *Phys. Rev. Res.* **2020**, *2*,

043369.

(34) Tang, S.; Habicht, A.; Li, S.; Seiffert, S.; Olsen, B. D. Self-Diffusion of Associating Star-Shaped Polymers. *Macromolecules* **2016**, *49* (15), 5599–5608.

(35) Rapp, P. B.; Omar, A. K.; Shen, J. J.; Buck, M. E.; Wang, Z. G.; Tirrell, D. A. Analysis and Control of Chain Mobility in Protein Hydrogels. *J. Am. Chem. Soc.* **2017**, *139* (10), 3796–3804.

(36) Rapp, P. B.; Omar, A. K.; Silverman, B. R.; Wang, Z.-G.; Tirrell, D. A. Mechanisms of Diffusion in Associative Polymer Networks: Evidence for Chain Hopping. *J. Am. Chem. Soc.* **2018**, *140*, 14185–14194.

(37) Ramirez, J.; Dursch, T. J.; Olsen, B. D. A Molecular Explanation for Anomalous Diffusion in Supramolecular Polymer Networks. *Macromolecules* **2018**, *51* (7), 2517–2525.

(38) Amin, D.; Likhtman, A. E.; Wang, Z. Dynamics in Supramolecular Polymer Networks Formed by Associating Telechelic Chains. *Macromolecules*. 2016, pp 7510–7524.

(39) Hoy, R. S.; Fredrickson, G. H. Thermoreversible Associating Polymer Networks. I. Interplay of Thermodynamics, Chemical Kinetics, and Polymer Physics. *J. Chem. Phys.* **2009**, *131*, 224902.

(40) Wang, R.; Alexander-Katz, A.; Johnson, J. A.; Olsen, B. D. Universal Cyclic Topology in Polymer Networks. *Phys. Rev. Lett.* **2016**, *116* (18), 1–5.

(41) Rossow, T.; Habicht, A.; Seiffert, S. Relaxation and Dynamics in Transient Polymer Model Networks. *Macromolecules*. 2014, pp 6473–6482.

(42) Sing, M. K.; Ramírez, J.; Olsen, B. D. Mechanical Response of Transient Telechelic Networks with Many-Part Stickers. *J. Chem. Phys.* **2017**, *147* (19), 1–19.

(43) De Gennes, P. G. *Scaling Concepts in Polymer Physics*; Cornell University Press, 1979.

(44) Guo, M.; Pitet, L. M.; Wyss, H. M.; Vos, M.; Dankers, P. Y. W.; Meijer, E. W. Tough Stimuli-Responsive Supramolecular Hydrogels with Hydrogen-Bonding Network Junctions. *J. Am. Chem. Soc.* **2014**, *136* (19), 6969–6977.

(45) Gillespie, D. T. Stochastic Simulation of Chemical Kinetics. *Annu. Rev. Phys. Chem.* **2007**, *58*, 35–55.

(46) Koslover, E. F.; Spakowitz, A. J. Multiscale Dynamics of Semiflexible Polymers from a Universal Coarse-Graining Procedure. *Phys. Rev. E - Stat. Nonlinear, Soft Matter Phys.* **2014**, *90* (1), 1–5.

(47) Gillespie, D. T. Approximate Accelerated Stochastic Simulation of Chemically Reacting Systems. *J. Chem. Phys.* **2001**, *115* (4), 1716–1733.

(48) Cao, Y.; Gillespie, D. T.; Petzold, L. R. Efficient Step Size Selection for the Tau-Leaping Simulation Method. *J. Chem. Phys.* **2006**, *124* (4), 1–11.

(49) Richter, D.; Stuhn, B.; Ewen, B.; Nerger, D. Collective Relaxation of Star Polymers - A Neutron Spin-Echo Study. *Phys. Rev. Lett.* **1987**, *58* (23), 2462–2465.

(50) Nava, G.; Rossi, M.; Biffi, S.; Sciortino, F.; Bellini, T. Fluctuating Elasticity Mode in Transient Molecular Networks. *Phys. Rev. Lett.* **2017**, *119* (7), 1–5.

(51) Doi, M.; Edwards, S. F. *The Theory of Polymer Dynamics*; Clarendon Press, 1988.

(52) Kumar, S. K.; Douglas, J. F. Gelation in Physically Associating Polymer Solutions. *Phys. Rev. Lett.* **2001**, *87* (18), 188301-1-188301–188304.

(53) Carrillo, J. Y.; Chen, W.; Wang, Z.; Sumpter, B. G.; Wang, Y. Chain Conformation of Polymer Melts with Associating Groups. *J. Phys. Commun.* **2019**, *3* (3), 35007.

(54) Rubinstein, M.; Semenov, A. N. Dynamics of Entangled Solutions of Associating Polymers. *Macromolecules* **2001**, *34* (4), 1058–1068.

(55) Ahmadi, M.; Hawke, L. G. D.; Goldansaz, H.; Van Ruymbeke, E. Dynamics of Entangled Linear Supramolecular Chains with Sticky Side Groups: Influence of Hindered Fluctuations. *Macromolecules* **2015**, *48* (19), 7300–7310.

(56) Lin, T. S.; Wang, R.; Johnson, J. A.; Olsen, B. D. Revisiting the Elasticity Theory for Real Gaussian Phantom Networks. *Macromolecules* **2019**, *52* (4), 1685–1694.

(57) James, H. M. Statistical Properties of Networks of Flexible Chains. *J. Chem. Phys.* **1947**, *15* (9), 651–668.

(58) Flory, P. J. Statistical Thermodynamics of Random Networks. *Proc R Soc London Ser A* **1976**, *351* (1666), 351–380.